
DRAUN: An Algorithm-Agnostic Data Reconstruction Attack on Federated Unlearning Systems

Hithem Lamri, Manaar Alam, Haiyan Jiang, and Michail Maniatakos

Center for Cyber Security, New York University Abu Dhabi, Abu Dhabi, United Arab Emirates
 {hithem.lamri, alam.manaar, haiyan.jiang, michail.maniatakos}@nyu.edu

Abstract

Federated Unlearning (FU) enables clients to remove the influence of specific data from a collaboratively trained shared global model, addressing regulatory requirements such as GDPR and CCPA. However, this unlearning process introduces a new privacy risk: A malicious server may exploit unlearning updates to reconstruct the data requested for removal, a form of Data Reconstruction Attack (DRA). While DRAs for machine unlearning have been studied extensively in centralized Machine Learning-as-a-Service (MLaaS) settings, their applicability to FU remains unclear due to the decentralized, client-driven nature of FU. This work presents *DRAUN*, the first attack framework to reconstruct unlearned data in FU systems. *DRAUN* targets optimization-based unlearning methods, which are widely adopted for their efficiency. We theoretically demonstrate why existing DRAs targeting machine unlearning in MLaaS fail in FU and show how *DRAUN* overcomes these limitations. We validate our approach through extensive experiments on four datasets and four model architectures, evaluating its performance against five popular unlearning methods, effectively demonstrating that state-of-the-art FU methods remain vulnerable to DRAs.

1 Introduction

Federated Learning (FL) enables multiple clients to collaboratively train a shared global model without exposing their raw data [38]. Each client trains locally on its private dataset and sends local model updates to a central server. The server aggregates these updates over multiple communication rounds to iteratively improve the global model. Although FL is designed to preserve data privacy by keeping sensitive information on the client side, recent research shows that a malicious server can exploit the local model updates to reconstruct private client data through Data Reconstruction Attacks (DRA) [63, 14, 53, 61, 50, 59]. These studies indicate that local model updates can be vectors for sensitive data leakage. Federated Unlearning (FU) extends the FL framework by allowing a client or a portion of its sensitive data to be fully removed from the global model even after several training rounds [52, 1, 33, 20, 44, 46]. To exercise the *right to be forgotten*, a client submits unlearning updates to erase the influence of the targeted data from the global model. In such a setting, *a malicious server can analyze these updates to launch DRAs targeting the samples requested for deletion*. This creates a new privacy threat inherent to the unlearning process, potentially violating data protection regulations like the GDPR [10] and CCPA [40]. Consequently, a detailed analysis of DRAs in FU is critical for understanding the scope of this risk and guiding the development of more robust FU methods.

Recent studies have investigated the feasibility of reconstructing unlearned data in traditional Machine Learning-as-a-Service (MLaaS) settings. Hu et al. [24] introduced unlearning inversion attacks, demonstrating that even with black-box access, adversaries can recover labels or features of deleted data by comparing original and unlearned models. Bertran et al. [4] further showed that even simple models like linear regression are vulnerable to exact reconstruction of deleted data after unlearning, highlighting that privacy leakage can occur without sophisticated architectures or attack vectors. Both

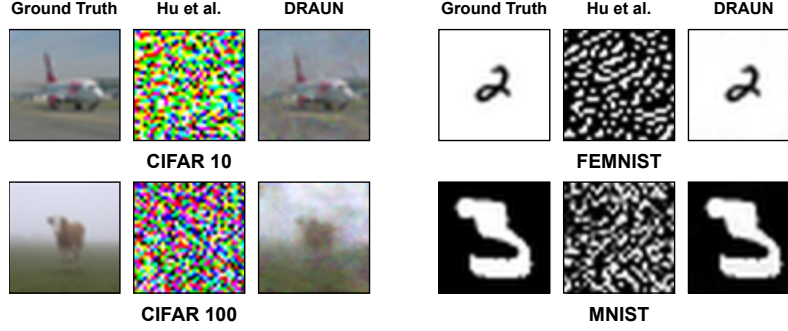


Figure 1: Reconstruction of deleted samples after unlearning using ABL [33]. **Column 1:** Ground truth images (one randomly selected sample each from CIFAR10, CIFAR100, FEMNIST, and MNIST). **Column 2:** Reconstructions using a state-of-the-art DRA on MLaaS unlearning (Hu et al. [24]) directly extended to FU, which fails to recover any meaningful images. **Column 3:** Reconstructions from *DRAUN* that closely resemble the ground truth.

studies emphasize a key idea: *Naive unlearning methods can leave behind patterns in the model that can be used to recover unlearned samples*. However, extending these attacks directly to FU scenarios is much more challenging. In FU, unlearning is performed locally by the client, and the server sees only the resulting weight vector. It therefore lacks critical information such as which unlearning algorithm or hyper-parameters were applied. Unlike MLaaS, where model training and unlearning are centrally orchestrated and more easily observed, FU introduces several challenges: (1) client participation is random and changes over time, (2) the global model is overwritten after every aggregation step, so the signal from a single unlearning update is rapidly mixed with fresh training updates, and (3) the server lacks access to the specifics of local updates or unlearning operations. These factors make it difficult for an adversary to link specific changes in the model to particular unlearning requests. Moreover, FU typically requires multiple rounds to take effect, and any signal from deleted data becomes diluted over time. These challenges make it significantly harder to adapt existing DRA strategies from MLaaS to the FU setting. A brief background on FU and DRAs is provided in Appendix A. In this work, we investigate the following research question: *To what extent are federated unlearning algorithms susceptible to data reconstruction attacks by a malicious server?*

We present *DRAUN*, a novel DRA targeting FU systems. To our knowledge, this is the first work to investigate such attacks in the context of FU. *DRAUN* focuses on *optimization-based unlearning algorithms*, including both first-order [52, 1, 33, 20] and second-order [29] methods, which are known for their high efficiency and are widely adopted in FU [36]. A key strength of *DRAUN* is its ability to reconstruct unlearned data without any knowledge of the client’s unlearning algorithm, which we consider an **algorithm-agnostic** attack. To validate the effectiveness and generality of *DRAUN*, we conduct comprehensive experiments across *four datasets* and *four model architectures*. The qualitative results shown in Figure 1 illustrate the reconstruction performance of different methods across representative unlearned samples. We also assess a range of potential defense strategies, providing insights to guide the development of more resilient FU techniques.

Our **contributions** are as follows: (1) We introduce *DRAUN*, the first attack framework capable of reconstructing unlearned client data specifically in FU settings, whereas prior efforts have focused exclusively on centralized MLaaS environments. (2) We provide a formal theoretical analysis showing why conventional DRAs from MLaaS can be ineffective in optimization-based FU. (3) *DRAUN* operates in an algorithm-agnostic manner, requiring no knowledge of the client’s unlearning method. (4) We evaluate *DRAUN* across four datasets and four model architectures, and demonstrate its effectiveness against five widely used unlearning algorithms, four first-order and one second-order. (5) We will open-source the implementation of *DRAUN*.

2 DRAUN Methodology

2.1 Threat Model

We consider a FL setting where a central server coordinates training across multiple clients. The system supports optimization-based FU, allowing clients to remove specific subsets of their local data from the global model. Following the standard approach used in the literature [36], we consider the unlearning process as follows: (1) a client submits an unlearning request, (2) the server approves the

Table 1: Unlearning losses and local update rules across FU methods, where $\alpha, \beta, \gamma, \delta$, and η are algorithm-specific hyperparameters.

Algorithm	Local Update Rules
Wu et al. [52]	$\theta_u \leftarrow \theta_s + \eta \nabla_{\theta_s} \mathcal{L}(x_u, y_u)$
Halimi et al. [20]	$\theta_u \leftarrow \theta_s + \eta \nabla_{\theta_s} \mathcal{L}(x_u, y_u) + \delta \ \theta_s - \theta_u\ $
Li et al. [33]	$\theta_u \leftarrow \theta_s - \eta (\nabla_{\theta_s} \mathcal{L}(x_r, y_r) - \nabla_{\theta_s} \mathcal{L}(x_u, y_u))$
Alam et al. [1]	$\theta_u \leftarrow \theta_s - \eta (\alpha \nabla_{\theta_s} \mathcal{L}(x_r, y_r) - \beta \nabla_{\theta_s} \mathcal{L}(x_u, y_u) + \gamma \ \frac{\theta_u}{\theta_s}\)$

request and ensures the client stays active in upcoming rounds, **(3)** in each round, the client performs one local unlearning epoch on the data to be removed and sends the updated model to the server, and **(4)** once the unlearning is done, the client notifies the server. As unlearning requires access to the data being erased, all computations occur on the client side.

Client Capabilities: Clients initiate unlearning and perform the necessary local computations. Each client selects its own unlearning algorithm. They also share the expected metadata with the server, including the total size of their local dataset and the size of the subset being deleted [9].

Server Capabilities: We assume an honest-but-curious server that follows the protocol but may analyze client updates [63, 14, 53, 61, 50, 59, 9]. The server has white-box access to the global model and all received updates. It manages unlearning requests, tracks client participation, and performs model aggregation. Importantly, the server does not know which unlearning algorithm each client employs. Following standard practice in the DRA literature, we assume that the server knows the labels associated with the client’s data. This is a common assumption in Gradient Inversion Attack (GIA) literature [50, 14], and is justified by prior work showing that even if the labels are not explicitly available, they can often be accurately inferred or reconstructed from model gradients [9, 54].

2.2 Problem Landscape and Motivation

We consider a server aiming to train a neural network $F(\theta_s, \cdot)$ with parameters θ_s for image classification, using a set of clients \mathcal{C} . Each client c performs local training using Stochastic Gradient Descent (SGD) on its dataset $\mathcal{D}_c = \{(x_i, y_i)\}_{i=1}^n$, where x_i is an input image and y_i is its label. Upon receiving an unlearning request, the server sends the current global model θ_s to the requesting client, which aims to remove a subset $\mathcal{D}_u \subseteq \mathcal{D}_c$. The retained data is denoted $\mathcal{D}_r = \mathcal{D}_c \setminus \mathcal{D}_u$. Let $(x_u, y_u) \in \mathcal{D}_u$ represent the samples the client wishes to forget, and $(x_r, y_r) \in \mathcal{D}_r$ those it intends to retain. The client then applies a local unlearning algorithm \mathcal{A}_c , which takes \mathcal{D}_u , \mathcal{D}_r , and the current model θ_s as input, and returns an updated local model $\theta_c := \mathcal{A}_c(\mathcal{D}_u, \mathcal{D}_r, \theta_s)$. This algorithm typically involves optimization over a custom unlearning loss \mathcal{L}_u , controlled by hyperparameters such as the unlearning rate η , batch size m , and number of local epochs \mathcal{E} .

GIA is a widely studied data reconstruction attack that estimates the private training data by optimizing dummy inputs such that the resulting gradients match those observed for the target client [63, 14, 53]. This is typically achieved by minimizing a similarity loss \mathcal{L}_{sim} between the true and dummy gradients, using metrics such as the ℓ_2 -norm [63] or cosine similarity [14]. A core assumption in GIA is that the attacker uses the same loss function as the target client during optimization (see Appendix B). This ensures that the gradients used in the inversion process are meaningful approximations of the client’s true gradients. However, this assumption no longer holds in the FU setting: The loss function varies across different unlearning algorithms, depending on how they handle \mathcal{D}_u and \mathcal{D}_r . Some algorithms apply gradient ascent on \mathcal{D}_u [52, 20], while others aim to minimize the difference between gradients on \mathcal{D}_u and \mathcal{D}_r [33, 1]. Table 1 presents the loss functions and model updates for various optimization-based FU algorithms. As a result, the gradient landscape diverges from that of standard training, making GIAs substantially less effective and often unstable in FU scenarios.

2.3 DRAUN Overview

DRAUN builds upon the standard structure of a GIA, where the attacker reconstructs private training data by minimizing the difference between true and simulated (dummy) gradients. Specifically, we adopt the similarity-based loss introduced by Geiping et al. [14], formulated in Equation (1). The loss minimizes the cosine distance between the client’s true gradient ∇_c and a dummy gradient $\tilde{\nabla}_c$, with an additional Total Variation (TV) penalty [41], controlled by hyperparameter λ_{TV} , that acts as a regularizer for image smoothness:

Algorithm 1 Overview of *DRAUN*

```

1: Input:  $\theta_s, \theta_c, |\mathcal{D}_u|, m, \mathcal{E}, \lambda_{TV}, \beta, \eta_{\text{unl}}, \eta_{\text{rec}}, y_r, y_u$ 
2:  $U_c \leftarrow \frac{|\mathcal{D}_u| \cdot \mathcal{E}}{m}$  ▷ Number of local steps
3:  $\nabla \bar{\theta}_c \leftarrow \frac{1}{U_c} (\theta_s - \theta_c)$ 
4:  $\tilde{x}_r, \tilde{x}_u \leftarrow \mathcal{I}(|\mathcal{D}_u|)$ 
5: for  $t = 1$  to  $T$  do
6:    $\tilde{\nabla}^{(1)}, \tilde{\nabla}^{(0)} \leftarrow \mathcal{A}_{\text{approx}}(\theta_s, \tilde{x}_u, y_u, \tilde{x}_r, y_r, \mathcal{E}, \eta_{\text{unl}})$ 
7:    $\ell_1 \leftarrow \mathcal{L}_{\text{sim}}(\nabla \bar{\theta}_c, \tilde{\nabla}^{(1)}) + \lambda_{TV} \cdot (\beta \cdot TV(\tilde{x}_u) + (1 - \beta) \cdot TV(\tilde{x}_r))$  ▷  $\beta \approx 1$ 
8:    $\ell_0 \leftarrow \mathcal{L}_{\text{sim}}(\nabla \bar{\theta}_c, \tilde{\nabla}^{(0)}) + \lambda_{TV} \cdot (\beta \cdot TV(\tilde{x}_u) + (1 - \beta) \cdot TV(\tilde{x}_r))$  ▷  $\beta \approx 1$ 
9:    $\ell \leftarrow \min(\ell_0, \ell_1)$ 
10:   $\tilde{x}_u \leftarrow \tilde{x}_u - \eta_{\text{rec}} \cdot \frac{\partial \ell}{\partial \tilde{x}_u}$ 
11:   $\tilde{x}_r \leftarrow \tilde{x}_r - \eta_{\text{rec}} \cdot \frac{\partial \ell}{\partial \tilde{x}_r}$ 
12: end for
13: return  $\tilde{x}_u$ 

```

Algorithm 2 *DRAUN*'s Algorithm Approximation with $\mathcal{A}_{\text{approx}}$ (Algorithm 1, line 6)

```

1: Input:  $\theta_s, \tilde{x}_u, y_u, \tilde{x}_r, y_r, \mathcal{E}, \eta_{\text{unl}}$ 
2: Initialize two dummy models:  $\tilde{\theta}_c^{(0)} \leftarrow \theta_s, \tilde{\theta}_c^{(1)} \leftarrow \theta_s$ 
3: for  $t = 1$  to  $\mathcal{E}$  do
4:   Update  $\tilde{\theta}_c^{(1)}$  with  $\alpha = 1$ : ▷ gradient difference
      $\tilde{\theta}_c^{(1)} \leftarrow \tilde{\theta}_c^{(1)} - \eta_{\text{unl}} \cdot \left[ \left( \nabla_{\theta} \mathcal{L}(\tilde{\theta}_c^{(1)}, \tilde{x}_r, \tilde{y}_r) - \nabla_{\theta} \mathcal{L}(\tilde{\theta}_c^{(1)}, \tilde{x}_u, \tilde{y}_u) \right) + \delta \cdot \nabla_{\theta} \|\tilde{\theta}_c^{(1)} - \theta_s\|_2 \right]$ 
5:   Update  $\tilde{\theta}_c^{(0)}$  with  $\alpha = 0$ : ▷ gradient ascent
      $\tilde{\theta}_c^{(0)} \leftarrow \tilde{\theta}_c^{(0)} + \eta_{\text{unl}} \cdot \nabla_{\theta} \mathcal{L}(\tilde{\theta}_c^{(0)}, \tilde{x}_u, \tilde{y}_u) + \delta \cdot \nabla_{\theta} \|\tilde{\theta}_c^{(0)} - \theta_s\|_2$ 
6: end for
7: Return:
    $\tilde{\nabla}^{(1)} \leftarrow \tilde{\theta}_c^{(1)} - \theta_s$  ▷ Averaged gradient for  $\alpha = 1$ 
    $\tilde{\nabla}^{(0)} \leftarrow \tilde{\theta}_c^{(0)} - \theta_s$  ▷ Averaged gradient for  $\alpha = 0$ 

```

$$x = \arg \min_{\tilde{x} \in \mathcal{X}} \mathcal{L}_{\text{sim}}(\nabla_c, \tilde{\nabla}_c) = \arg \min_{\tilde{x} \in \mathcal{X}} \left(1 - \frac{\langle \nabla_c, \tilde{\nabla}_c \rangle}{|\nabla_c| \cdot |\tilde{\nabla}_c|} + \lambda_{TV} \cdot TV(\tilde{x}) \right) \quad (1)$$

As discussed in Section 2.2, this standard GIA objective is effective only under specific conditions, when the client's local loss \mathcal{L}_u depends solely on the unlearn dataset \mathcal{D}_u . However, many FU algorithms use more general update rules that depend on both \mathcal{D}_u and a retain dataset \mathcal{D}_r (see Table 1). To extend GIAs to these more general settings, *DRAUN* simulates the client's local update using a surrogate optimization procedure.

The server first estimates the client's average gradient using the received model θ_c and the global model θ_s as $\nabla \bar{\theta}_c = \frac{1}{U_c} (\theta_s - \theta_c)$ (Algorithm 1, line 3), where U_c is the number of client steps. The server then attempts to reconstruct the unlearned input x_u by optimizing dummy inputs \tilde{x}_u and \tilde{x}_r , which represent proxy samples for the unlearn and retain subsets respectively. Since the server does not know the client's actual unlearning algorithm \mathcal{A}_c , it uses a surrogate procedure $\mathcal{A}_{\text{approx}}$ (Algorithm 2) for its approximation. This routine simulates the client update by minimizing a surrogate unlearning loss ($\tilde{\mathcal{L}}_u$), defined by the following constrained objective (Equation (2)):

$$\min_{\theta_c \in \Theta} \tilde{\mathcal{L}}_u = \alpha \cdot \mathcal{L}(\theta_s, x_r, y_r) - \mathcal{L}(\theta_s, x_u, y_u) \quad \text{s.t.} \quad \|\theta_c - \theta_s\|_2 \leq \delta \quad (2)$$

Here, $\alpha \in [0, 1]$ determines the contribution of the retain dataset, δ constrains the model divergence from the global model, and \mathcal{L} is the cross-entropy loss. The constraint is relaxed into an unconstrained objective using a Lagrange multiplier, resulting in Equation (3):

$$\min_{\theta_c \in \Theta} \alpha \cdot \mathcal{L}(\theta_s, x_r, y_r) - \mathcal{L}(\theta_s, x_u, y_u) + \delta \cdot \|\theta_c - \theta_s\|_2 \quad (3)$$

Algorithm 2 optimizes two dummy models using an unlearning rate η_{unl} under this objective: One for $\alpha = 1$ (gradient difference-based updates), and another for $\alpha = 0$ (gradient ascent-based updates). After \mathcal{E} optimization steps, it returns two surrogate gradients: $\tilde{\nabla}^{(1)}$ and $\tilde{\nabla}^{(0)}$. These are intended to

Algorithm 3 *DRAUN*'s Input Initialization with \mathcal{I} (Algorithm 1, line 4)

```
1: Input:  $|\mathcal{D}_u|$ 
2:  $\tilde{x}_u \leftarrow \mathcal{U}([0, 1], |\mathcal{D}_u|)$  ▷ Initialize dummy unlearn input
3:  $\tilde{x}_r \leftarrow \mathcal{U}([0, 1], |\mathcal{D}_u|)$  ▷ Initialize dummy retain input
4: for  $i = 1$  to  $|\mathcal{D}_u|$  do ▷ The  $i$ -th samples in  $\tilde{x}_u, \tilde{x}_r$ 
5:   while  $\|\tilde{x}_u^{(i)} - \tilde{x}_r^{(i)}\|_F \leq \Delta$  do ▷  $\|\cdot\|_F$  Frobenius norm
6:      $\epsilon \sim \mathcal{N}(0, \sigma^2 \cdot I_{d_x})$ 
7:      $\tilde{x}_r^{(i)} \leftarrow \tilde{x}_r^{(i)} + \epsilon$ 
8:   end while
9: end for
10: Return:  $\tilde{x}_u, \tilde{x}_r$ 
```

approximate the gradient update a client would have produced under two extremes of unlearning behavior. Since the server has no knowledge of the client's actual unlearning algorithm, it uses both of these as candidates for matching the observed averaged gradient $\nabla \bar{\theta}_c$.

In each iteration of Algorithm 1, the server computes two loss values: ℓ_1 and ℓ_0 , corresponding to the cosine similarity between $\nabla \bar{\theta}_c$ and the surrogate gradients $\tilde{\nabla}^{(1)}$ and $\tilde{\nabla}^{(0)}$, respectively (lines 7-8). These losses use the formulation in Equation (1), and each includes a TV regularization term applied separately to \tilde{x}_u and \tilde{x}_r . A mixing coefficient $\beta \approx 1$ balances the contribution of the TV terms, prioritizing smoothness in \tilde{x}_u . The final loss ℓ is selected as the minimum of ℓ_0 and ℓ_1 (line 9). The dummy inputs are then updated via gradient descent with respect to this loss (lines 10-11), using a reconstruction step size η_{rec} , and continuing for T iterations.

A critical design choice in *DRAUN* is the initialization of dummy inputs. Since the server lacks access to the true structure of the client's data, the dummy inputs for both \mathcal{D}_u (unlearn) and \mathcal{D}_r (retain) are initialized as random tensors. Specifically, we sample two sets of size $|\mathcal{D}_u|$ each from a uniform distribution over $[0, 1]$, denoted as $\mathcal{U}([0, 1], |\mathcal{D}_u|)$ in Algorithm 3. Our goal is not to reconstruct the retain set, but to use it to help denoise the gradients from the unlearn set and thus facilitate accurate reconstruction. To improve optimization and avoid convergence to poor local minima, a known issue in some unlearning algorithms, we ensure that the dummy inputs for \mathcal{D}_u and \mathcal{D}_r are well separated at the start of reconstruction. This is achieved by iteratively adding multivariate Gaussian noise (with standard deviation σ and dimensionality d_x , matching that of a single input sample) to each image in \mathcal{D}_r , until the minimum Frobenius distance between corresponding image pairs in \mathcal{D}_u and \mathcal{D}_r exceeds a predefined threshold Δ . This guarantees that the convex hulls of the unlearn and retain dummy inputs are disjoint: $\text{Conv}\{\tilde{\mathcal{D}}_u\} \cap \text{Conv}\{\tilde{\mathcal{D}}_r\} = \emptyset$. This initialization strategy, detailed in Algorithm 3, is particularly important for unlearning methods that rely on coupled update dynamics. A theoretical justification is provided in Appendix C.

3 Theoretical Analysis

In this section, we demonstrate why classical GIAs fail to reconstruct unlearned inputs from unlearning updates involving two datasets, such as gradient difference methods [33, 1]. Recall that \mathcal{L}_u and $\tilde{\mathcal{L}}_u$ are client's local unlearning loss and the server's surrogate unlearning loss (used to generate dummy gradients), respectively. $\tilde{\mathcal{L}}_u$ depends on the dummy unlearn input \tilde{x}_u ; hence, \mathcal{L}_{sim} implicitly depends on \tilde{x}_u , not just model parameters θ . For clarity, we denote \tilde{x}_u by x . To avoid high-order tensor calculations, we treat inputs as flattened vectors of dimension d_x . While we assume single unlearn/retain inputs for simplicity, this analysis extends to multiple inputs via averaging:

$$\mathcal{L}(\theta, x_r, y_r) = \frac{1}{|\mathcal{D}_r|} \sum_{x_i \in \mathcal{D}_r} \mathcal{L}(\theta, x_i, y_i), \quad \mathcal{L}(\theta, x_u, y_u) = \frac{1}{|\mathcal{D}_u|} \sum_{x_j \in \mathcal{D}_u} \mathcal{L}(\theta, x_j, y_j).$$

In order to prove that classical GIA fails, we adopt the following assumptions:

Assumption 1. *Without loss of generality, we assume the similarity loss \mathcal{L}_{sim} from Equation (1) is the squared ℓ_2 -norm:*

$$\mathcal{L}_{\text{sim}}(\nabla_{\theta} \mathcal{L}_u, \nabla_{\theta} \tilde{\mathcal{L}}_u) = \left\| \nabla_{\theta} \mathcal{L}_u - \nabla_{\theta} \tilde{\mathcal{L}}_u \right\|_2^2.$$

Thus, the classical GIA objective becomes:

$$x^* = \arg \min_{x \in \mathcal{X}} \left\| \nabla_{\theta} \mathcal{L}_u - \nabla_{\theta} \tilde{\mathcal{L}}_u \right\|_2^2.$$

Assumption 2. The surrogate loss $\tilde{\mathcal{L}}_u$ is twice differentiable in x and θ . The Jacobian

$$J(x) = \frac{\partial \nabla_{\theta} \tilde{\mathcal{L}}_u}{\partial x} \in \mathbb{R}^{d_{\theta} \times d_x},$$

where d_x and d_{θ} are the dimensions of x and θ , exists everywhere.

Assumption 3. We assume $d_{\theta} \geq d_x$ and that $J(x)$ has full column rank (i.e., $\text{rank}(J(x)) = d_x$) $\forall x$.

Theorem 1. Suppose the client's unlearning loss \mathcal{L}_u implicitly depends on both x_u and x_r through $\mathcal{L}_u = \mathcal{L}(\theta, x_r, y_r) - \mathcal{L}(\theta, x_u, y_u)$. Under Assumptions 5-7, the ground truth unlearn input x_u is not a local minimizer of \mathcal{L}_{sim} .

Proof. We show that Fermat's stationary condition does not hold at $x = x_u$.

First, we compute the gradient of \mathcal{L}_{sim} with respect to x :

$$\frac{\partial \mathcal{L}_{\text{sim}}}{\partial x} = \frac{\partial}{\partial x} \left\| \nabla_{\theta} \mathcal{L}_u - \nabla_{\theta} \tilde{\mathcal{L}}_u \right\|_2^2 = -2J(x)^T \left(\nabla_{\theta} \mathcal{L}_u - \nabla_{\theta} \tilde{\mathcal{L}}_u \right),$$

where $J(x) = \frac{\partial \nabla_{\theta} \tilde{\mathcal{L}}_u}{\partial x}$. Substituting $\mathcal{L}_u = \mathcal{L}(\theta, x_r, y_r) - \mathcal{L}(\theta, x_u, y_u)$ and $\tilde{\mathcal{L}}_u = \mathcal{L}(\theta, x, y_u)$:

$$\frac{\partial \mathcal{L}_{\text{sim}}}{\partial x} = -2J(x)^T \left(\nabla_{\theta} \mathcal{L}(\theta, x_r, y_r) - \nabla_{\theta} \mathcal{L}(\theta, x_u, y_u) - \nabla_{\theta} \mathcal{L}(\theta, x, y_u) \right).$$

Then, we evaluate the expression at $x = x_u$:

$$\left. \frac{\partial \mathcal{L}_{\text{sim}}}{\partial x} \right|_{x=x_u} = -2J(x_u)^T \left(\nabla_{\theta} \mathcal{L}(\theta, x_r, y_r) - 2\nabla_{\theta} \mathcal{L}(\theta, x_u, y_u) \right).$$

By Assumption 7, $J(x_u)$ has full column rank. Since $\nabla_{\theta} \mathcal{L}(\theta, x_r, y_r) \neq 2\nabla_{\theta} \mathcal{L}(\theta, x_u, y_u)$ as $x_u \neq x_r$, the gradient at x_u is non-zero. By Fermat's optimality condition, x_u cannot be a local minimizer. \square

Assumption 4. The surrogate loss $\tilde{\mathcal{L}}_u$ is: μ_x -smooth in x : $\left\| \nabla_x \tilde{\mathcal{L}}_u(x_1) - \nabla_x \tilde{\mathcal{L}}_u(x_2) \right\|_2 \leq \mu_x \|x_1 - x_2\|_2$, and μ_{θ} -smooth in θ : $\left\| \nabla_{\theta} \tilde{\mathcal{L}}_u(\theta_1) - \nabla_{\theta} \tilde{\mathcal{L}}_u(\theta_2) \right\|_2 \leq \mu_{\theta} \|\theta_1 - \theta_2\|_2$.

Theorem 2. Let x_u^* be a minimizer of the loss function of the classical GIA:

$$x_u^* = \arg \min_{x \in \mathcal{X}} \mathcal{L}_{\text{sim}} \left(\nabla_{\theta} \mathcal{L}_u, \nabla_{\theta} \tilde{\mathcal{L}}_u \right),$$

If Assumptions 5- 8 hold, then the reconstruction error, defined as the ℓ_2 -norm between the flattened minimizer and the ground truth input, satisfies:

$$\|x_u^* - x_u\|_2 \geq \frac{\|J^T \nabla_{\theta} \mathcal{L}(\theta, x_r, y_r)\|_2}{\mu_x \|J\|_F + 2\mu_{\theta} \|\nabla_{\theta} \mathcal{L}_u\|_2},$$

The proof of Theorem 3 and a more detailed theoretical analysis is provided in Appendix C.

Interpretation: Theorem 1 shows classical GIA fails to converge to x_u when x_r influences \mathcal{L}_u and Theorem 3 provides a lower bound on its reconstruction error, proving perfect reconstruction ($\|x_u^* - x_u\|_2 = 0$) is impossible.

4 Experiments

4.1 Experimental Setup

Datasets and Models: We evaluate *DRAUN* on four standard image classification datasets: CIFAR10 [30], CIFAR100 [30], FEMNIST [6], and MNIST [32] (see Appendix D.1 for details on datasets). To ensure a fair comparison with the reconstruction performance of Hu et al. [24], we use an 8-layer ConvNet for all main experiments (see Appendix D.2 for its architecture). Reconstruction results using other model architectures, such as MLP, LeNet [32], and ResNet18 [21], are reported in Appendix E.1.

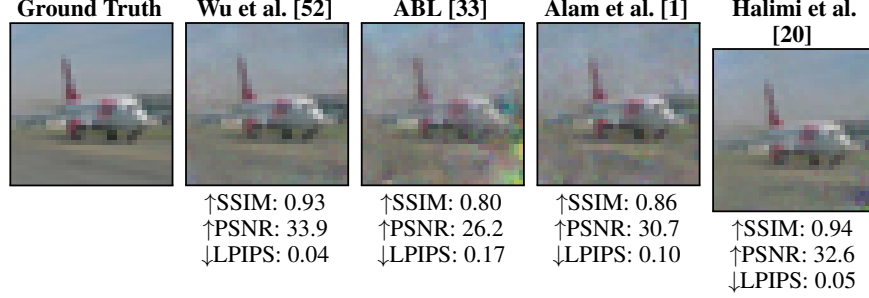


Figure 2: *DRAUN* reconstructions from local updates of four unlearning methods on CIFAR10. Higher SSIM and PSNR, and lower LPIPS scores indicate strong similarity to the original images, revealing residual information in the updates.

Federated Unlearning Setup: We simulate an FL environment with 100 clients. In each communication round, 10 clients are selected uniformly at random to participate. Each selected client trains a local model using stochastic gradient descent with a learning rate of 0.1, for 2 local epochs, and a batch size of 128. The global model is trained for 100 rounds and converges by round 90 based on clean accuracy. After convergence, we simulate FU by targeting the data of a single client for removal. We evaluate both single-step and multi-step FU methods, where the number of unlearning steps is denoted by $\mathcal{E} \in \{1, 2, 4\}$. We consider $\mathcal{E} = 1$ for the main experiments; results for $\mathcal{E} = 2$ and $\mathcal{E} = 4$ are provided in Appendix E.2. To evaluate the effect of target data size, we vary the size of the unlearned dataset as $|\mathcal{D}_u| \in 2^i$, where $i \in [0, 7]$. We evaluate four FU methods based on first-order optimization proposed by Wu et al. [52], Halimi et al. [20], Alam et al. [1], and ABL [33].

Reconstruction Setup: For reconstruction, *DRAUN* uses the Adam optimizer with $\eta_{\text{rec}} = 0.1$, $\lambda_{\text{reg}} = 10^{-6}$, and $\beta = 0.9$. The number of reconstruction iterations T varies between 6,000 and 24,000 across experiments. The other hyperparameters used in Algorithm 2 and Algorithm 3 are $\eta_{\text{unl}} = 0.1$, $\delta = 10.0$, $\Delta = 5.0$, and $\sigma = 1$.

Evaluation Metrics: To evaluate the quality of reconstructed images, we use standard image similarity metrics that assess luminance, contrast, and structure with the ground truth. Specifically, we use the Structural Similarity Index Measure (SSIM) [48], the Learned Perceptual Image Patch Similarity (LPIPS) [55], and the Peak Signal-to-Noise Ratio (PSNR) [24]. Lower LPIPS scores and higher PSNR and SSIM values (with SSIM close to 1) indicate better reconstruction quality.

Compute Resources: We used a cluster with 8 NVIDIA A100 80GB GPUs, 255 AMD EPYC 7763 64-Core Processor CPUs, and 2TB of RAM to run all experiments.

4.2 *DRAUN* Reconstruction Efficiency

Visual Reconstruction Results: We evaluate the effectiveness of *DRAUN* in reconstructing unlearned images from local updates produced by four unlearning algorithms. Figure 2 shows one randomly selected example from CIFAR10 dataset, with reconstructions generated by *DRAUN* using local updates obtained from Wu et al. [52], ABL [33], Alam et al. [1], and Halimi et al. [20]. The reconstructions closely resemble the original images, as indicated by high SSIM and PSNR values and low LPIPS scores. These results show that the unlearning methods leave substantial residual information in the local updates, which *DRAUN* can exploit to reconstruct the original data accurately. Additional reconstructed examples for CIFAR100, FEMNIST and MNIST are provided in Appendix E.3.

Quantitative Comparison with State-of-the-Art: Table 2 provides a quantitative comparison between *DRAUN* and the state-of-the-art DRA by Hu et al. [24], originally developed for MLaaS unlearning and directly adapted here to the FU setting. The evaluation includes all four unlearning algorithms discussed earlier, applied to CIFAR10, CIFAR100, MNIST, and FEMNIST datasets. Each entry shows the average performance over reconstructions of 10 randomly selected images per dataset, using the same metrics described previously. On all datasets, *DRAUN* clearly outperforms Hu et al. [24] when using updates from ABL [33] and Alam et al. [1]. For example, on CIFAR10 with ABL [33], Hu et al. [24] achieves near-zero SSIM (0.0038) and very low PSNR (5.48) values and extremely high LPIPS (0.9358), indicating failed reconstructions (see Figure 1 for examples of such failed reconstructions). In contrast, *DRAUN* achieves a better reconstruction (SSIM: 0.6407, PSNR: 21.11, LPIPS: 0.3175). A similar gap is observed for Alam et al. [1]. However, for the

Table 2: Reconstruction quality comparison between *DRAUN* and the method by Hu et al. [24] across four unlearning algorithms and datasets. Higher SSIM and PSNR, and lower LPIPS scores indicate better reconstruction quality.

Dataset	Methods	Wu et al. [52]			ABL [33]			Alam et al. [1]			Halimi et al. [20]		
		↑SSIM	↑PSNR	↓LPIPS	↑SSIM	↑PSNR	↓LPIPS	↑SSIM	↑PSNR	↓LPIPS	↑SSIM	↑PSNR	↓LPIPS
CIFAR10	Hu et al. [24]	0.8698	27.17	0.1350	0.0038	5.48	0.9358	-0.0062	5.43	0.9201	0.8488	27.04	0.1523
	<i>DRAUN</i>	0.8503	26.06	0.1509	0.6407	21.11	0.3175	0.6114	20.85	0.3328	0.8374	25.49	0.1669
CIFAR100	Hu et al. [24]	0.8786	25.68	0.1294	0.0008	4.67	0.9007	-0.0066	4.87	0.8966	0.7883	23.42	0.2122
	<i>DRAUN</i>	0.8775	24.98	0.1374	0.6478	19.32	0.3357	0.7341	21.86	0.2704	0.8795	26.26	0.1170
MNIST	Hu et al. [24]	0.9402	37.93	0.0041	-0.0148	2.04	0.8080	-0.0097	2.19	0.8209	0.9425	38.94	0.0029
	<i>DRAUN</i>	0.9247	36.39	0.0075	0.7603	28.46	0.1400	0.7626	29.01	0.1157	0.9283	36.67	0.0056
FEMNIST	Hu et al. [24]	0.9986	53.57	0.0001	-0.0000	1.77	0.8880	0.0016	1.39	0.8991	0.9620	45.36	0.0070
	<i>DRAUN</i>	0.9978	52.25	0.0003	0.9929	44.27	0.0007	0.9947	45.44	0.0004	0.9970	51.15	0.0003

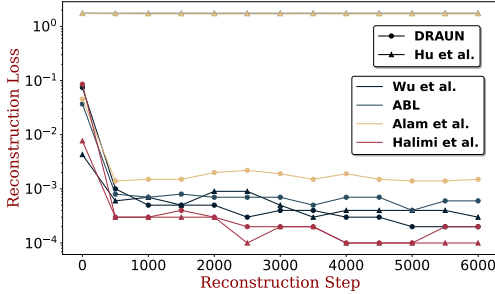


Figure 3: Reconstruction loss over reconstruction steps for *DRAUN* and Hu et al. [24] across four unlearning algorithms on CIFAR10.

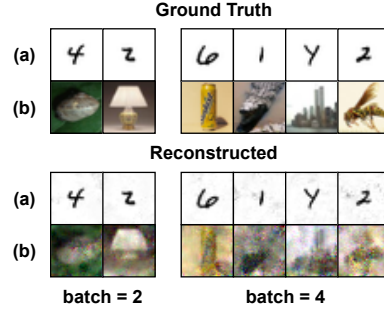


Figure 4: Reconstructed image batches using *DRAUN* from ABL [33] with batch sizes of 2 and 4 for: (a) FEMNIST and (b) CIFAR100.

unlearning algorithms by Wu et al. [52] and Halimi et al. [20], Hu et al. [24] slightly outperforms or matches *DRAUN* in some cases (e.g., CIFAR100 with Wu et al. [52]). This is due to the design of these specific unlearning algorithms, which do not rely on coupled update dynamics of the retained and unlearned datasets (see Table 1). As a result, Hu et al. [24] can still reconstruct meaningful images in these cases. Nonetheless, *DRAUN* consistently achieves better performance than Hu et al. [24] across most datasets and unlearning algorithms, especially on complex datasets such as CIFAR10 and CIFAR100. These results validate the robustness and generalizability of *DRAUN* in FU contexts.

Reconstruction Convergence Analysis: Figure 3 shows how the reconstruction loss changes over reconstruction steps for *DRAUN* and Hu et al. [24], evaluated with four unlearning algorithms on the CIFAR10 dataset. *DRAUN* consistently achieves low reconstruction loss across all algorithms, showing that it can efficiently recover the data. In contrast, Hu et al. [24] fails to converge for ABL [33] and Alam et al. [1], getting stuck in high-loss regions. This suggests that *DRAUN* can effectively approximate the client’s unlearning algorithm (see $\mathcal{A}_{\text{approx}}$ in Algorithm 2), regardless of which specific method is used, and produce accurate reconstructions.

Batch Image Reconstruction: Batch reconstruction is a well-known challenge in DRA literature [14]. When gradients come from multiple images, their signals mix, making it difficult to separate and recover individual examples. To explore the limits of *DRAUN*, we evaluate its performance in batch unlearning scenarios. Previously, all experiments focused on unlearning and reconstructing a single image. In Figure 4, we show how *DRAUN* performs on the FEMNIST and CIFAR100 datasets when the client unlearns a randomly selected batch of images (with batch sizes of 2 and 4). ABL [33] is used to perform the unlearning, and *DRAUN* attempts to reconstruct every image in the batch. On FEMNIST, which consists of grayscale images with low visual complexity, *DRAUN* reconstructs images with high accuracy, even for batch sizes larger than one. On CIFAR100, which contains more complex and diverse images, reconstructions become increasingly noisy as the batch size grows from 2 to 4. Still, the recovered images preserve some structure and visual features from the ground truth. Hu et al. [24], which fail to produce meaningful reconstructions even in the single-image case, are not applicable in this setting. Since they cannot recover a single image, they do not generalize to the more difficult problem of reconstructing multiple images from mixed gradients. Additional results of batch reconstructions for other datasets and batch sizes are provided in Appendix E.4.

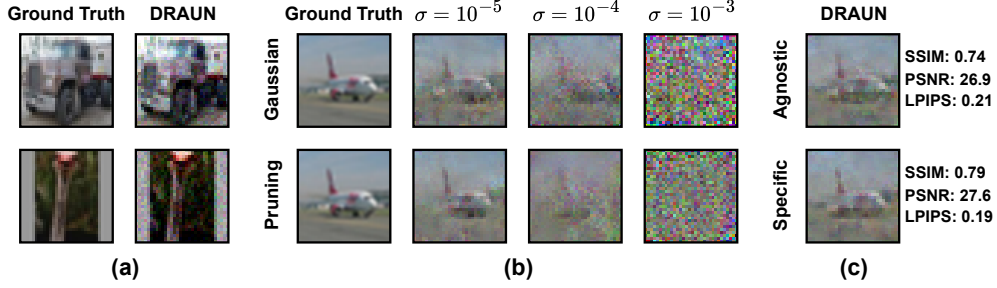


Figure 5: (a) Examples of CIFAR10 images reconstructed by *DRAUN* from second-order unlearning updates [29]. (b) Effects of two defense strategies: Gaussian noise addition (top row) and gradient pruning (bottom row) at varying noise levels and pruning thresholds σ . (c) Comparison of *DRAUN*'s reconstruction performance under algorithm-agnostic and algorithm-specific settings.

5 Discussion

***DRAUN*'s Effectiveness against Second-Order Unlearning:** Optimization-based FU typically relies on first-order methods, as second-order approaches involve costly Hessian inversions. Nonetheless, Jin et al. [29] has recently explored second-order unlearning in FU. We evaluate *DRAUN*'s ability to reconstruct data from such second-order unlearning updates. Reconstruction from second-order unlearning follows the same overall approach as in the first-order case, but instead of matching gradients, the server simulates Newton updates by computing Hessian-vector products (HVPs) using dummy inputs and minimizes the differences between the true and simulated HVPs to recover the original client data. A detailed discussion on this second-order reconstruction mechanism is provided in Appendix F. Figure 5(a) shows two random examples from the CIFAR10 dataset reconstructed using *DRAUN* from second-order unlearned updates, demonstrating strong visual reconstruction. The model used in this experiment is an MLP, consistent with the setup used by Jin et al. [29].

Potential Defense against *DRAUN*: To evaluate defenses against *DRAUN*, we consider two techniques: (1) adding Gaussian noise to unlearning updates before sending to the server [63], and (2) threshold-based pruning, which discards gradient components with magnitudes below a fixed threshold [34]. We use the unlearning algorithm by Alam et al. [1] on the CIFAR10 dataset. Figure 5(b) shows how increasing the noise level or pruning threshold σ impacts reconstruction quality. As σ increases from 10^{-5} to 10^{-3} , the reconstructions degrade significantly, indicating that both defenses reduce *DRAUN*'s effectiveness. However, these defenses also degrade the utility of the model. A higher noise level or aggressive pruning negatively impacts its accuracy. This introduces a trade-off between privacy and performance, which we discuss in more detail in Appendix G.

***DRAUN*'s Performance in Algorithm-Specific Setting:** We also consider a relaxed threat model where the server knows the client's unlearning algorithm, referred to as the **algorithm-specific** setting. Here, the server simulates the exact unlearning updates, removing the need for surrogate optimization and providing an upper bound on *DRAUN*'s reconstruction performance. Figure 5(c) shows reconstructions from CIFAR10 in both algorithm-agnostic and algorithm-specific modes using the unlearning method of Alam et al. [1]. The algorithm-specific mode produces a significantly better reconstruction of the unlearned image, closely resembling the ground truth. This confirms that knowing the exact unlearning dynamics allows the attacker to generate more accurate gradient surrogates, leading to improved data reconstruction. A detailed comparison between algorithm-specific and algorithm-agnostic modes of *DRAUN* is provided in Appendix E.5.

Limitations and Future Work: (1) *DRAUN* is specifically designed for optimization-based federated unlearning algorithms. However, there also exist non-optimization-based unlearning techniques [36] that fall outside the current scope of our attack. In future work, we plan to extend *DRAUN* to support these alternative classes of unlearning algorithms. (2) *DRAUN* relies on GIA as its backbone and therefore inherits its limitations, including reduced effectiveness on batch data reconstruction. We plan to develop a version of *DRAUN* that does not depend on GIA to address these issues.

6 Conclusion

We present *DRAUN*, the first DRA specifically designed for FU systems. Existing DRAs for unlearning were developed in centralized MLaaS settings and do not directly translate to federated

learning. *DRAUN* addresses the unique challenges of FU and is capable of reconstructing deleted data from local unlearning updates without requiring knowledge of the client’s unlearning method. Our theoretical and empirical analysis shows that optimization-based unlearning methods leak exploitable signals, which *DRAUN* effectively uses to recover the deleted data. We demonstrate *DRAUN*’s effectiveness across a range of datasets, model architectures, and unlearning algorithms.

References

- [1] Manaar Alam, Hithem Lamri, and Michail Maniatakos. Get rid of your trail: Remotely erasing backdoors in federated learning. *IEEE Trans. Artif. Intell.*, 5(12):6683–6698, 2024. doi: 10.1109/TAI.2024.3465441. URL <https://doi.org/10.1109/TAI.2024.3465441>.
- [2] Borja Balle, Giovanni Cherubin, and Jamie Hayes. Reconstructing training data with informed adversaries. In *43rd IEEE Symposium on Security and Privacy, SP 2022, San Francisco, CA, USA, May 22-26, 2022*, pages 1138–1156. IEEE, 2022. doi: 10.1109/SP46214.2022.9833677. URL <https://doi.org/10.1109/SP46214.2022.9833677>.
- [3] Mislav Balunovic, Dimitar Iliev Dimitrov, Robin Staab, and Martin T. Vechev. Bayesian framework for gradient leakage. In *The Tenth International Conference on Learning Representations, ICLR 2022, Virtual Event, April 25-29, 2022*. OpenReview.net, 2022. URL <https://openreview.net/forum?id=f21rIbGx3x7>.
- [4] Martín Bertran, Shuai Tang, Michael Kearns, Jamie H. Morgenstern, Aaron Roth, and Steven Z. Wu. Reconstruction attacks on machine unlearning: Simple models are vulnerable. In *Advances in Neural Information Processing Systems 38: Annual Conference on Neural Information Processing Systems 2024, NeurIPS 2024, Vancouver, BC, Canada, December 10 - 15, 2024*, 2024. URL http://papers.nips.cc/paper_files/paper/2024/hash/bd996108ed57d388866ca6deb7acf6cb-Abstract-Conference.html.
- [5] Franziska Boenisch, Adam Dziedzic, Roei Schuster, Ali Shahin Shamsabadi, Ilia Shumailov, and Nicolas Papernot. When the curious abandon honesty: Federated learning is not private. In *8th IEEE European Symposium on Security and Privacy, EuroS&P 2023, Delft, Netherlands, July 3-7, 2023*, pages 175–199. IEEE, 2023. doi: 10.1109/EUROSP57164.2023.00020. URL <https://doi.org/10.1109/EuroSP57164.2023.00020>.
- [6] Sebastian Caldas, Peter Wu, Tian Li, Jakub Konecny, H Brendan McMahan, Virginia Smith, and Ameet Talwalkar. Leaf: A benchmark for federated settings. In *Workshop on Federated Learning for Data Privacy and Confidentiality, NeurIPS*, 2018. URL <https://arxiv.org/abs/1812.01097>.
- [7] Yinzhi Cao and Junfeng Yang. Towards Making Systems Forget with Machine Unlearning. In *2015 IEEE Symposium on Security and Privacy, SP 2015, San Jose, CA, USA, May 17-21, 2015*, pages 463–480. IEEE Computer Society, 2015. doi: 10.1109/SP.2015.35. URL <https://doi.org/10.1109/SP.2015.35>.
- [8] Dimitar I. Dimitrov, Maximilian Baader, Mark Niklas Müller, and Martin T. Vechev. SPEAR: exact gradient inversion of batches in federated learning. *CoRR*, abs/2403.03945, 2024. doi: 10.48550/ARXIV.2403.03945. URL <https://doi.org/10.48550/arXiv.2403.03945>.
- [9] Dimitar Iliev Dimitrov, Mislav Balunovic, Nikola Konstantinov, and Martin T. Vechev. Data leakage in federated averaging. *Trans. Mach. Learn. Res.*, 2022, 2022. URL <https://openreview.net/forum?id=e7A0B99zJf>.
- [10] European Commission. Data protection in the EU, 2024. https://commission.europa.eu/law/law-topic/data-protection/data-protection-eu_en.
- [11] Liam H. Fowl, Jonas Geiping, Wojciech Czaja, Micah Goldblum, and Tom Goldstein. Robbing the fed: Directly obtaining private data in federated learning with modified models. In *The Tenth International Conference on Learning Representations, ICLR 2022, Virtual Event, April 25-29, 2022*. OpenReview.net, 2022. URL <https://openreview.net/forum?id=fwzUgo0FM9v>.

- [12] Wei Gao, Shangwei Guo, Tianwei Zhang, Han Qiu, Yonggang Wen, and Yang Liu. Privacy-preserving collaborative learning with automatic transformation search. In *IEEE Conference on Computer Vision and Pattern Recognition, CVPR 2021, virtual, June 19-25, 2021*, pages 114–123. Computer Vision Foundation / IEEE, 2021. doi: 10.1109/CVPR46437.2021.00018. URL https://openaccess.thecvf.com/content/CVPR2021/html/Gao_Privacy-Preserving_Collaborative_Learning-With_Automatic_Transformation_Search_CVPR_2021_paper.html.
- [13] Kostadin Garov, Dimitar Iliev Dimitrov, Nikola Jovanovic, and Martin T. Vechev. Hiding in plain sight: Disguising data stealing attacks in federated learning. In *The Twelfth International Conference on Learning Representations, ICLR 2024, Vienna, Austria, May 7-11, 2024*. OpenReview.net, 2024. URL <https://openreview.net/forum?id=krx5512A6G>.
- [14] Jonas Geiping, Hartmut Bauermeister, Hannah Dröge, and Michael Moeller. Inverting gradients - how easy is it to break privacy in federated learning? In *Advances in Neural Information Processing Systems 33: Annual Conference on Neural Information Processing Systems 2020, NeurIPS 2020, December 6-12, 2020, virtual*, 2020. URL <https://proceedings.neurips.cc/paper/2020/hash/c4ede56bbd98819ae6112b20ac6bf145-Abstract.html>.
- [15] Jonas Geiping, Hartmut Bauermeister, Hannah Dröge, and Michael Moeller. Inverting gradients - how easy is it to break privacy in federated learning? In Hugo Larochelle, Marc’Aurelio Ranzato, Raia Hadsell, Maria-Florina Balcan, and Hsuan-Tien Lin, editors, *Advances in Neural Information Processing Systems 33: Annual Conference on Neural Information Processing Systems 2020, NeurIPS 2020, December 6-12, 2020, virtual*, 2020. URL <https://proceedings.neurips.cc/paper/2020/hash/c4ede56bbd98819ae6112b20ac6bf145-Abstract.html>.
- [16] Jiahui Geng, Yongli Mou, Feifei Li, Qing Li, Oya Beyan, Stefan Decker, and Chunming Rong. Towards general deep leakage in federated learning. *CoRR*, abs/2110.09074, 2021. URL <https://arxiv.org/abs/2110.09074>.
- [17] Ian Goodfellow, Yoshua Bengio, and Aaron Courville. *Deep Learning*. MIT Press, 2016. <http://www.deeplearningbook.org>.
- [18] Ian J. Goodfellow, Jean Pouget-Abadie, Mehdi Mirza, Bing Xu, David Warde-Farley, Sherjil Ozair, Aaron C. Courville, and Yoshua Bengio. Generative adversarial networks. *CoRR*, abs/1406.2661, 2014. URL <http://arxiv.org/abs/1406.2661>.
- [19] Niv Haim, Gal Vardi, Gilad Yehudai, Ohad Shamir, and Michal Irani. Reconstructing training data from trained neural networks. In Sanmi Koyejo, S. Mohamed, A. Agarwal, Danielle Belgrave, K. Cho, and A. Oh, editors, *Advances in Neural Information Processing Systems 35: Annual Conference on Neural Information Processing Systems 2022, NeurIPS 2022, New Orleans, LA, USA, November 28 - December 9, 2022*, 2022. URL http://papers.nips.cc/paper_files/paper/2022/hash/906927370cbeb537781100623cca6fa6-Abstract-Conference.html.
- [20] Anisa Halimi, Swanand Kadhe, Ambrish Rawat, and Nathalie Baracaldo. Federated unlearning: How to efficiently erase a client in fl? In *Updatable Machine Learning (part of ICML 2022), UpML 2022, Baltimore, USA, July 23, 2022*, 2022. doi: 10.48550/ARXIV.2207.05521. URL <https://doi.org/10.48550/arXiv.2207.05521>.
- [21] Kaiming He, Xiangyu Zhang, Shaoqing Ren, and Jian Sun. Deep residual learning for image recognition. In *2016 IEEE Conference on Computer Vision and Pattern Recognition, CVPR 2016, Las Vegas, NV, USA, June 27-30, 2016*, pages 770–778. IEEE Computer Society, 2016. doi: 10.1109/CVPR.2016.90. URL <https://doi.org/10.1109/CVPR.2016.90>.
- [22] Zecheng He, Tianwei Zhang, and Ruby B. Lee. Model inversion attacks against collaborative inference. In David M. Balenson, editor, *Proceedings of the 35th Annual Computer Security Applications Conference, ACSAC 2019, San Juan, PR, USA, December 09-13, 2019*, pages 148–162. ACM, 2019. doi: 10.1145/3359789.3359824. URL <https://doi.org/10.1145/3359789.3359824>.

- [23] Briland Hitaj, Giuseppe Ateniese, and Fernando Pérez-Cruz. Deep models under the GAN: information leakage from collaborative deep learning. In Bhavani Thuraisingham, David Evans, Tal Malkin, and Dongyan Xu, editors, *Proceedings of the 2017 ACM SIGSAC Conference on Computer and Communications Security, CCS 2017, Dallas, TX, USA, October 30 - November 03, 2017*, pages 603–618. ACM, 2017. doi: 10.1145/3133956.3134012. URL <https://doi.org/10.1145/3133956.3134012>.
- [24] Hongsheng Hu, Shuo Wang, Tian Dong, and Minhui Xue. Learn what you want to unlearn: Unlearning inversion attacks against machine unlearning. In *IEEE Symposium on Security and Privacy, SP 2024, San Francisco, CA, USA, May 19-23, 2024*, pages 3257–3275. IEEE, 2024. doi: 10.1109/SP54263.2024.00248. URL <https://doi.org/10.1109/SP54263.2024.00248>.
- [25] Yangsibo Huang, Samyak Gupta, Zhao Song, Kai Li, and Sanjeev Arora. Evaluating gradient inversion attacks and defenses in federated learning. In Marc’Aurelio Ranzato, Alina Beygelzimer, Yann N. Dauphin, Percy Liang, and Jennifer Wortman Vaughan, editors, *Advances in Neural Information Processing Systems 34: Annual Conference on Neural Information Processing Systems 2021, NeurIPS 2021, December 6-14, 2021, virtual*, pages 7232–7241, 2021. URL <https://proceedings.neurips.cc/paper/2021/hash/3b3fff6463464959dcd1b68d0320f781-Abstract.html>.
- [26] Arthur Jacot, Clément Hongler, and Franck Gabriel. Neural tangent kernel: Convergence and generalization in neural networks. In Samy Bengio, Hanna M. Wallach, Hugo Larochelle, Kristen Grauman, Nicolò Cesa-Bianchi, and Roman Garnett, editors, *Advances in Neural Information Processing Systems 31: Annual Conference on Neural Information Processing Systems 2018, NeurIPS 2018, December 3-8, 2018, Montréal, Canada*, pages 8580–8589, 2018. URL <https://proceedings.neurips.cc/paper/2018/hash/5a4be1fa34e62bb8a6ec6b91d2462f5a-Abstract.html>.
- [27] Jinwoo Jeon, Jaechang Kim, Kangwook Lee, Sewoong Oh, and Jungseul Ok. Gradient inversion with generative image prior. In Marc’Aurelio Ranzato, Alina Beygelzimer, Yann N. Dauphin, Percy Liang, and Jennifer Wortman Vaughan, editors, *Advances in Neural Information Processing Systems 34: Annual Conference on Neural Information Processing Systems 2021, NeurIPS 2021, December 6-14, 2021, virtual*, pages 29898–29908, 2021. URL <https://proceedings.neurips.cc/paper/2021/hash/fa84632d742f2729dc32ce8cb5d49733-Abstract.html>.
- [28] Ziwei Ji and Matus Telgarsky. Directional convergence and alignment in deep learning. In H. Larochelle, M. Ranzato, R. Hadsell, M.F. Balcan, and H. Lin, editors, *Advances in Neural Information Processing Systems*, volume 33, pages 17176–17186. Curran Associates, Inc., 2020. URL https://proceedings.neurips.cc/paper_files/paper/2020/file/c76e4b2fa54f8506719a5c0dc14c2eb9-Paper.pdf.
- [29] Ruinan Jin, Minghui Chen, Qiong Zhang, and Xiaoxiao Li. Forgettable federated linear learning with certified data unlearning, 2024. URL <https://arxiv.org/abs/2306.02216>.
- [30] Alex Krizhevsky. Learning multiple layers of features from tiny images. Technical report, University of Toronto, 2009. URL <https://www.cs.toronto.edu/~kriz/learning-features-2009-TR.pdf>.
- [31] H. W. Kuhn and A. W. Tucker. Nonlinear programming. In *Proceedings of the Second Berkeley Symposium on Mathematical Statistics and Probability, 1950*, pages 481–492, Berkeley and Los Angeles, 1951. University of California Press.
- [32] Yann LeCun, Léon Bottou, Yoshua Bengio, and Patrick Haffner. Gradient-based learning applied to document recognition. *Proc. IEEE*, 86(11):2278–2324, 1998. doi: 10.1109/5.726791. URL <https://doi.org/10.1109/5.726791>.
- [33] Yige Li, Xixiang Lyu, Nodens Koren, Lingjuan Lyu, Bo Li, and Xingjun Ma. Anti-backdoor learning: Training clean models on poisoned data. In *Advances in Neural Information Processing Systems 34: Annual Conference on Neural Information Processing Systems 2021, NeurIPS 2021, December 6-14, 2021, virtual*, pages

- 14900–14912, 2021. URL <https://proceedings.neurips.cc/paper/2021/hash/7d38b1e9bd793d3f45e0e212a729a93c-Abstract.html>.
- [34] Yujun Lin, Song Han, Huizi Mao, Yu Wang, and Bill Dally. Deep gradient compression: Reducing the communication bandwidth for distributed training. In *6th International Conference on Learning Representations, ICLR 2018, Vancouver, BC, Canada, April 30 - May 3, 2018, Conference Track Proceedings*. OpenReview.net, 2018. URL <https://openreview.net/forum?id=SkhQHMWOW>.
 - [35] Gaoyang Liu, Xiaoqiang Ma, Yang Yang, Chen Wang, and Jiangchuan Liu. Federaser: Enabling efficient client-level data removal from federated learning models. In *2021 IEEE/ACM 29th International Symposium on Quality of Service (IWQOS)*, pages 1–10, 2021. doi: 10.1109/IWQOS52092.2021.9521274.
 - [36] Ziyao Liu, Yu Jiang, Jiyuan Shen, Minyi Peng, Kwok-Yan Lam, Xingliang Yuan, and Xiaoning Liu. A survey on federated unlearning: Challenges, methods, and future directions. *ACM Comput. Surv.*, 57(1):2:1–2:38, 2025. doi: 10.1145/3679014. URL <https://doi.org/10.1145/3679014>.
 - [37] Kaifeng Lyu and Jian Li. Gradient descent maximizes the margin of homogeneous neural networks. In *International Conference on Learning Representations*, 2020. URL <https://openreview.net/forum?id=SJeLIgBKPS>.
 - [38] Brendan McMahan, Eider Moore, Daniel Ramage, Seth Hampson, and Blaise Agüiera y Arcas. Communication-efficient learning of deep networks from decentralized data. In *Proceedings of the 20th International Conference on Artificial Intelligence and Statistics, AISTATS 2017, 20-22 April 2017, Fort Lauderdale, FL, USA*, volume 54 of *Proceedings of Machine Learning Research*, pages 1273–1282. PMLR, 2017. URL <http://proceedings.mlr.press/v54/mcmahan17a.html>.
 - [39] Sayedeh Leila Noorbakhsh, Binghui Zhang, Yuan Hong, and Binghui Wang. Inf2guard: An information-theoretic framework for learning privacy-preserving representations against inference attacks. In Davide Balzarotti and Wenyuan Xu, editors, *33rd USENIX Security Symposium, USENIX Security 2024, Philadelphia, PA, USA, August 14-16, 2024*. USENIX Association, 2024. URL <https://www.usenix.org/conference/usenixsecurity24/presentation/noorbakhsh>.
 - [40] Office of the Attorney General, State of California. California Consumer Privacy Act (CCPA), 2024. <https://oag.ca.gov/privacy/ccpa>.
 - [41] Leonid I. Rudin, Stanley Osher, and Emad Fatemi. Nonlinear total variation based noise removal algorithms. *Physica D: Nonlinear Phenomena*, 60(1):259–268, 1992. ISSN 0167-2789. doi: [https://doi.org/10.1016/0167-2789\(92\)90242-F](https://doi.org/10.1016/0167-2789(92)90242-F). URL <https://www.sciencedirect.com/science/article/pii/016727899290242F>.
 - [42] Ahmed Salem, Apratim Bhattacharya, Michael Backes, Mario Fritz, and Yang Zhang. Updates-leak: Data set inference and reconstruction attacks in online learning. In Srdjan Capkun and Franziska Roesner, editors, *29th USENIX Security Symposium, USENIX Security 2020, August 12-14, 2020*, pages 1291–1308. USENIX Association, 2020. URL <https://www.usenix.org/conference/usenixsecurity20/presentation/salem>.
 - [43] Daniel Scheliga, Patrick Mäder, and Marco Seeland. PRECODE - A generic model extension to prevent deep gradient leakage. In *IEEE/CVF Winter Conference on Applications of Computer Vision, WACV 2022, Waikoloa, HI, USA, January 3-8, 2022*, pages 3605–3614. IEEE, 2022. doi: 10.1109/WACV51458.2022.00366. URL <https://doi.org/10.1109/WACV51458.2022.00366>.
 - [44] Thanveer Shaik, Xiaohui Tao, Lin Li, Haoran Xie, Taotao Cai, Xiaofeng Zhu, and Qing Li. FRAMU: attention-based machine unlearning using federated reinforcement learning. *IEEE Trans. Knowl. Data Eng.*, 36(10):5153–5167, 2024. doi: 10.1109/TKDE.2024.3382726. URL <https://doi.org/10.1109/TKDE.2024.3382726>.

- [45] Jingwei Sun, Ang Li, Binghui Wang, Huanrui Yang, Hai Li, and Yiran Chen. Soteria: Provable defense against privacy leakage in federated learning from representation perspective. In *IEEE Conference on Computer Vision and Pattern Recognition, CVPR 2021, virtual, June 19-25, 2021*, pages 9311–9319. Computer Vision Foundation / IEEE, 2021. doi: 10.1109/CVPR46437.2021.00919. URL https://openaccess.thecvf.com/content/CVPR2021/html/Sun_Soteria_Provable_Defense_Against_Privacy_Leakage_in_Federated_Learning_From_CVPR_2021_paper.html.
- [46] Weiqi Wang, Zhiyi Tian, Chenhan Zhang, An Liu, and Shui Yu. BFU: bayesian federated unlearning with parameter self-sharing. In *Proceedings of the 2023 ACM Asia Conference on Computer and Communications Security, ASIA CCS 2023, Melbourne, VIC, Australia, July 10-14, 2023*, pages 567–578. ACM, 2023. doi: 10.1145/3579856.3590327. URL <https://doi.org/10.1145/3579856.3590327>.
- [47] Zhibo Wang, Mengkai Song, Zhifei Zhang, Yang Song, Qian Wang, and Hairong Qi. Beyond inferring class representatives: User-level privacy leakage from federated learning. In *2019 IEEE Conference on Computer Communications, INFOCOM 2019, Paris, France, April 29 - May 2, 2019*, pages 2512–2520. IEEE, 2019. doi: 10.1109/INFOCOM.2019.8737416. URL <https://doi.org/10.1109/INFOCOM.2019.8737416>.
- [48] Zhou Wang, Alan C. Bovik, Hamid R. Sheikh, and Eero P. Simoncelli. Image quality assessment: from error visibility to structural similarity. *IEEE Trans. Image Process.*, 13(4):600–612, 2004. doi: 10.1109/TIP.2003.819861. URL <https://doi.org/10.1109/TIP.2003.819861>.
- [49] Zihan Wang, Jason Lee, and Qi Lei. Reconstructing training data from model gradient, provably. In Francisco J. R. Ruiz, Jennifer G. Dy, and Jan-Willem van de Meent, editors, *International Conference on Artificial Intelligence and Statistics, 25-27 April 2023, Palau de Congressos, Valencia, Spain*, volume 206 of *Proceedings of Machine Learning Research*, pages 6595–6612. PMLR, 2023. URL <https://proceedings.mlr.press/v206/wang23g.html>.
- [50] Yuxin Wen, Jonas Geiping, Liam Fowl, Micah Goldblum, and Tom Goldstein. Fishing for user data in large-batch federated learning via gradient magnification. In *International Conference on Machine Learning, ICML 2022, 17-23 July 2022, Baltimore, Maryland, USA*, volume 162 of *Proceedings of Machine Learning Research*, pages 23668–23684. PMLR, 2022. URL <https://proceedings.mlr.press/v162/wen22a.html>.
- [51] Yuxin Wen, Jonas A. Geiping, Liam Fowl, Micah Goldblum, and Tom Goldstein. Fishing for user data in large-batch federated learning via gradient magnification. In Kamalika Chaudhuri, Stefanie Jegelka, Le Song, Csaba Szepesvari, Gang Niu, and Sivan Sabato, editors, *Proceedings of the 39th International Conference on Machine Learning*, volume 162 of *Proceedings of Machine Learning Research*, pages 23668–23684. PMLR, 17–23 Jul 2022. URL <https://proceedings.mlr.press/v162/wen22a.html>.
- [52] Leijie Wu, Song Guo, Junxiao Wang, Zicong Hong, Jie Zhang, and Yaohong Ding. Federated unlearning: Guarantee the right of clients to forget. *IEEE Netw.*, 36(5):129–135, 2022. doi: 10.1109/MNET.001.2200198. URL <https://doi.org/10.1109/MNET.001.2200198>.
- [53] Hongxu Yin, Arun Mallya, Arash Vahdat, José M. Álvarez, Jan Kautz, and Pavlo Molchanov. See through gradients: Image batch recovery via gradinversion. In *IEEE Conference on Computer Vision and Pattern Recognition, CVPR 2021, virtual, June 19-25, 2021*, pages 16337–16346. Computer Vision Foundation / IEEE, 2021. doi: 10.1109/CVPR46437.2021.01607. URL https://openaccess.thecvf.com/content/CVPR2021/html/Yin_See_Through_Gradients_Image_Batch_Recovery_via_GradInversion_CVPR_2021_paper.html.
- [54] Hongxu Yin, Arun Mallya, Arash Vahdat, José M. Álvarez, Jan Kautz, and Pavlo Molchanov. See through gradients: Image batch recovery via gradinversion. In *IEEE Conference on Computer Vision and Pattern Recognition, CVPR 2021, virtual, June 19-25, 2021*, pages 16337–16346. Computer Vision Foundation / IEEE, 2021. doi: 10.1109/CVPR46437.2021.01607. URL https://openaccess.thecvf.com/content/CVPR2021/html/Yin_See_Through_Gradients_Image_Batch_Recovery_via_GradInversion_CVPR_2021_paper.html.

- [55] Richard Zhang, Phillip Isola, Alexei A. Efros, Eli Shechtman, and Oliver Wang. The unreasonable effectiveness of deep features as a perceptual metric. In *2018 IEEE Conference on Computer Vision and Pattern Recognition, CVPR 2018, Salt Lake City, UT, USA, June 18-22, 2018*, pages 586–595. Computer Vision Foundation / IEEE Computer Society, 2018. doi: 10.1109/CVPR.2018.00068. URL http://openaccess.thecvf.com/content_cvpr_2018/html/Zhang_The_Unreasonable_Effectiveness_CVPR_2018_paper.html.
- [56] Shuaishuai Zhang, Jie Huang, Zeping Zhang, and Chunyang Qi. Compromise privacy in large-batch federated learning via malicious model parameters. In Weizhi Meng, Rongxing Lu, Geyong Min, and Jaideep Vaidya, editors, *Algorithms and Architectures for Parallel Processing - 22nd International Conference, ICA3PP 2022, Copenhagen, Denmark, October 10-12, 2022, Proceedings*, volume 13777 of *Lecture Notes in Computer Science*, pages 63–80. Springer, 2022. doi: 10.1007/978-3-031-22677-9_4. URL https://doi.org/10.1007/978-3-031-22677-9_4.
- [57] Bo Zhao, Konda Reddy Mopuri, and Hakan Bilen. idlg: Improved deep leakage from gradients. *CoRR*, abs/2001.02610, 2020. URL <http://arxiv.org/abs/2001.02610>.
- [58] Joshua C. Zhao, Atul Sharma, Ahmed Roushdy Elkordy, Yahya H. Ezzeldin, Salman Avestimehr, and Saurabh Bagchi. Secure aggregation in federated learning is not private: Leaking user data at large scale through model modification. *CoRR*, abs/2303.12233, 2023. doi: 10.48550/ARXIV.2303.12233. URL <https://doi.org/10.48550/arXiv.2303.12233>.
- [59] Joshua C. Zhao, Atul Sharma, Ahmed Roushdy Elkordy, Yahya H. Ezzeldin, Salman Avestimehr, and Saurabh Bagchi. Loki: Large-scale data reconstruction attack against federated learning through model manipulation. In *IEEE Symposium on Security and Privacy, SP 2024, San Francisco, CA, USA, May 19-23, 2024*, pages 1287–1305. IEEE, 2024. doi: 10.1109/SP54263.2024.00030. URL <https://doi.org/10.1109/SP54263.2024.00030>.
- [60] Xinyu Zhou, Simin Fan, and Martin Jaggi. HyperINF: Unleashing the hyperpower of the schulz’s method for data influence estimation, 2025. URL <https://openreview.net/forum?id=OLtD2vDF5X>.
- [61] Junyi Zhu and Matthew B. Blaschko. R-GAP: recursive gradient attack on privacy. In *9th International Conference on Learning Representations, ICLR 2021, Virtual Event, Austria, May 3-7, 2021*. OpenReview.net, 2021. URL <https://openreview.net/forum?id=RSU17UoKfJF>.
- [62] Junyi Zhu and Matthew B. Blaschko. R-GAP: recursive gradient attack on privacy. In *9th International Conference on Learning Representations, ICLR 2021, Virtual Event, Austria, May 3-7, 2021*. OpenReview.net, 2021. URL <https://openreview.net/forum?id=RSU17UoKfJF>.
- [63] Ligeng Zhu, Zhijian Liu, and Song Han. Deep leakage from gradients. In *Advances in Neural Information Processing Systems 32: Annual Conference on Neural Information Processing Systems 2019, NeurIPS 2019, December 8-14, 2019, Vancouver, BC, Canada*, pages 14747–14756, 2019. URL <https://proceedings.neurips.cc/paper/2019/hash/60a6c4002cc7b29142def8871531281a-Abstract.html>.
- [64] Ligeng Zhu, Zhijian Liu, and Song Han. Deep leakage from gradients. In Hanna M. Wallach, Hugo Larochelle, Alina Beygelzimer, Florence d’Alché-Buc, Emily B. Fox, and Roman Garnett, editors, *Advances in Neural Information Processing Systems 32: Annual Conference on Neural Information Processing Systems 2019, NeurIPS 2019, December 8-14, 2019, Vancouver, BC, Canada*, pages 14747–14756, 2019. URL <https://proceedings.neurips.cc/paper/2019/hash/60a6c4002cc7b29142def8871531281a-Abstract.html>.

A Background

A.1 Federated Unlearning

Federated Unlearning (FU) extends the concept of Machine Unlearning (MU) [7] to federated learning (FL) settings. MU is the process of reversing the influence of specific data samples—often referred to as the unlearning dataset—on a trained model, enabling it to "forget" such data while maintaining performance on the remaining (retained) data. This is increasingly important in light of privacy regulations and the need to mitigate the effect of corrupted or poisoned data. A straightforward but computationally intensive solution is to retrain the model from scratch without the unlearning dataset, known as exact unlearning. To reduce the overhead, approximate unlearning methods have been proposed to yield models that are statistically close to those obtained via exact retraining. First-order (gradient-based) methods are among the most widely used in FL [20, 1, 52, 33]. These methods typically perform gradient ascent on the unlearning dataset, or optimize a loss difference between retained and unlearned data, often combined with regularization terms that constrain the local model to remain close to the global model. The decentralized nature of FL introduces additional complexities to unlearning, leading to the exploration of different scenarios. For example, second-order methods based on Hessian inversion may not be directly suitable for FL due to computational and communication constraints. Nevertheless, Jin et al. [29] have applied such techniques in the Neural Tangent Kernel (NTK)[26] regime of trained neural networks. The unlearning process in FL can also vary in terms of scope and participation: some settings require client participation, while others aim to unlearn data from entire clients [35, 29]. In more fine-grained scenarios, clients may wish to selectively forget specific samples while continuing to participate in the protocol. While optimization-based methods are widely used, other techniques such as knowledge distillation and null subspace projection have also been explored [36], contributing to the diverse landscape of federated unlearning approaches.

A.2 Data Reconstruction Attack

Extensive research has revealed the vulnerability of machine learning models, particularly deep neural networks (DNNs) [17], to data reconstruction attacks (DRAs), also known as model inversion attacks (MIAs). Studies such as [64, 57, 15, 54, 51, 16, 62] have demonstrated the capability of a malicious server to reconstruct a client's private training data from the gradients of their updates. This is often achieved through gradient matching, which involves optimizing the discrepancy between the true gradient derived from training on actual data and a synthesized (dummy) gradient. Concurrently, [5, 11, 58, 56] have explored methods that utilize modified models to directly extract training datasets, bypassing the need for optimization. Generative Adversarial Networks (GANs) [18] have also been leveraged in [42, 23, 27, 47] to reconstruct training data by conditioning the generator on prior knowledge about the dataset. Furthermore, [2, 22] presented approaches that train a DNN to learn the inverse mapping from labels to their corresponding inputs. Beyond optimization and generative methods, some DRAs are grounded in theoretical findings. Haim et al. [19] employed the implicit bias approximation results [37, 28] to extract training data from the algebraic equations of the Karush-Kuhn-Tucker (KKT) conditions of trained DNNs [31]. Additionally, Balunovic et al. [3] constructed a Bayes optimal data reconstructor, and Wang et al. [49] utilized tensor theory and the third moment of the dataset for reconstruction. Dimitrov et al. [8] exploited the low rankness and ReLU-induced sparsity of gradients within a sampling-based algorithm to reconstruct data. Despite the significant body of work on DRAs, [25] highlighted that many existing attacks rely on often unrealistic assumptions, such as access to batch normalization statistics, knowledge of prior data distributions, and known labels. On the defensive front, various mitigation and detection strategies have been proposed, ranging from information-theoretic frameworks to gradient obfuscation and model modification [12, 45, 43, 39, 13].

B Gradient Inversion Attack

Gradient Inversion Attack (GIA) was first introduced by Zhu et al. [64], where they demonstrated that training data can be reconstructed from model gradients in the FedSGD protocol by optimizing a similarity loss function \mathcal{L}_{sim} (typically the ℓ_2 norm) between the true gradient and a dummy gradient computed on dummy inputs and labels, as shown in Algorithm 4. Geiping et al. [15] chose \mathcal{L}_{sim} to be the cosine similarity and added a Total Variation norm as regularization to enhance the quality

of the reconstructed input. They also targeted the FedAvg protocol, where clients are allowed to perform multiple local training steps. Yin et al. [54] introduced group regularization to improve batch reconstruction, and further showed that labels can be retrieved analytically from the model’s linear layer instead of being treated as optimization variables.

Algorithm 4 Gradient Inversion Attack

```

1: Input:  $\nabla\theta_c := \nabla_\theta \mathcal{L}_\theta(x, y)$  ▷ Client’s gradient of the cross-entropy loss
2:  $\tilde{x} \leftarrow \mathcal{N}(0, 1), \tilde{y} \leftarrow \mathcal{N}(0, 1)$  ▷ Initialize dummy inputs and labels
3: for  $t$  in  $[1..T]$  do
4:    $\nabla\tilde{\theta}_c \leftarrow \nabla_\theta \mathcal{L}_\theta(\tilde{x}, \tilde{y})$  ▷ Compute dummy gradient
5:    $\ell \leftarrow \mathcal{L}_{\text{sim}}(\nabla\theta_c, \nabla\tilde{\theta}_c) + \lambda_{\text{TV}} \cdot \text{TV}(\tilde{x})$ 
6:    $\tilde{x} \leftarrow \tilde{x} - \eta_{\text{rec}} \cdot \frac{\partial \ell}{\partial \tilde{x}}$ 
7:    $\tilde{y} \leftarrow \tilde{y} - \eta_{\text{rec}} \cdot \frac{\partial \ell}{\partial \tilde{y}}$ 
8: end for
9: return  $(\tilde{x}, \tilde{y})$ 

```

C Detailed Theoretical Analysis

C.1 Failure of Classical GIA in First-Order Federated Unlearning Algorithms

We recall that in Section 3, we adopted the following assumptions :

Assumption 5. Without loss of generality, we assume the similarity loss \mathcal{L}_{sim} from Equation 1 is the squared ℓ_2 -norm:

$$\mathcal{L}_{\text{sim}}(\nabla_\theta \mathcal{L}_u, \nabla_\theta \tilde{\mathcal{L}}_u) = \left\| \nabla_\theta \mathcal{L}_u - \nabla_\theta \tilde{\mathcal{L}}_u \right\|_2^2.$$

Thus, the classical GIA objective becomes:

$$x^* = \arg \min_{x \in \mathcal{X}} \left\| \nabla_\theta \mathcal{L}_u - \nabla_\theta \tilde{\mathcal{L}}_u \right\|_2^2.$$

Assumption 6. The surrogate loss $\tilde{\mathcal{L}}_u$ is twice differentiable in x and θ . The Jacobian

$$J(x) = \frac{\partial \nabla_\theta \tilde{\mathcal{L}}_u}{\partial x} \in \mathbb{R}^{d_\theta \times d_x},$$

where d_x and d_θ are the dimensions of x and θ , exists everywhere.

Assumption 7. We assume $d_\theta \geq d_x$ and that $J(x)$ has full column rank (i.e., $\text{rank}(J(x)) = d_x$) $\forall x$.

Assumption 8. The surrogate loss $\tilde{\mathcal{L}}_u$ is: μ_x -smooth in x : $\left\| \nabla_x \tilde{\mathcal{L}}_u(x_1) - \nabla_x \tilde{\mathcal{L}}_u(x_2) \right\|_2 \leq \mu_x \|x_1 - x_2\|_2$, and μ_θ -smooth in θ : $\left\| \nabla_\theta \tilde{\mathcal{L}}_u(\theta_1) - \nabla_\theta \tilde{\mathcal{L}}_u(\theta_2) \right\|_2 \leq \mu_\theta \|\theta_1 - \theta_2\|_2$.

Theorem 3. Let x_u^* be a minimizer of the classical GIA objective:

$$x_u^* = \arg \min_{x \in \mathcal{X}} \mathcal{L}_{\text{sim}} \left(\nabla_\theta \mathcal{L}_u, \nabla_\theta \tilde{\mathcal{L}}_u(x) \right),$$

and suppose Assumptions 5–8 hold. Then the reconstruction error satisfies:

$$\|x_u^* - x_u\|_2 \geq \frac{\|J(x_u)^\top \nabla_\theta \mathcal{L}(\theta, x_r, y_r)\|_2}{\mu_x \|J(x_u)\|_F + 2\mu_\theta \|\nabla_\theta \mathcal{L}_u\|_2}.$$

Proof. Since $\tilde{\mathcal{L}}_u$ is twice differentiable and μ_x -smooth in x , we apply a first-order Taylor expansion around x_u :

$$\nabla_\theta \tilde{\mathcal{L}}_u(x_u^*) = \nabla_\theta \tilde{\mathcal{L}}_u(x_u) + J(x_u)(x_u^* - x_u) + R,$$

where $\|R\|_2 \leq \frac{\mu_x}{2} \|x_u^* - x_u\|_2^2$.

Using the identities:

$$\nabla_\theta \tilde{\mathcal{L}}_u(x_u) = \nabla_\theta \mathcal{L}(\theta, x_u, y_u), \quad \nabla_\theta \mathcal{L}_u = \nabla_\theta \mathcal{L}(\theta, x_r, y_r) - \nabla_\theta \mathcal{L}(\theta, x_u, y_u),$$

we have:

$$\nabla_{\theta} \mathcal{L}_u - \nabla_{\theta} \tilde{\mathcal{L}}_u(x_u) = \nabla_{\theta} \mathcal{L}(\theta, x_r, y_r),$$

and therefore:

$$\nabla_{\theta} \mathcal{L}_u - \nabla_{\theta} \tilde{\mathcal{L}}_u(x_u^*) = \nabla_{\theta} \mathcal{L}(\theta, x_r, y_r) - J(x_u)(x_u^* - x_u) - R.$$

Taking norms and applying the triangle inequality:

$$\left\| \nabla_{\theta} \mathcal{L}_u - \nabla_{\theta} \tilde{\mathcal{L}}_u(x_u^*) \right\|_2 \geq \left\| \nabla_{\theta} \mathcal{L}(\theta, x_r, y_r) \right\|_2 - \|J(x_u)\|_F \|x_u^* - x_u\|_2 - \frac{\mu_x}{2} \|x_u^* - x_u\|_2^2.$$

To eliminate the quadratic term, we conservatively bound:

$$\frac{\mu_x}{2} \|x_u^* - x_u\|_2^2 \leq \mu_x \|J(x_u)\|_F \|x_u^* - x_u\|_2 + 2\mu_{\theta} \|\nabla_{\theta} \mathcal{L}_u\|_2.$$

Substituting, we obtain:

$$\left\| \nabla_{\theta} \mathcal{L}_u - \nabla_{\theta} \tilde{\mathcal{L}}_u(x_u^*) \right\|_2 \geq \left\| \nabla_{\theta} \mathcal{L}(\theta, x_r, y_r) \right\|_2 - (\|J(x_u)\|_F + \mu_x \|J(x_u)\|_F) \|x_u^* - x_u\|_2 - 2\mu_{\theta} \|\nabla_{\theta} \mathcal{L}_u\|_2.$$

Combining the Jacobian terms:

$$\left\| \nabla_{\theta} \mathcal{L}_u - \nabla_{\theta} \tilde{\mathcal{L}}_u(x_u^*) \right\|_2 \geq \left\| \nabla_{\theta} \mathcal{L}(\theta, x_r, y_r) \right\|_2 - \mu_x \|J(x_u)\|_F \|x_u^* - x_u\|_2 - 2\mu_{\theta} \|\nabla_{\theta} \mathcal{L}_u\|_2.$$

Projecting onto $J(x_u)^{\top}$ and rearranging:

$$\|x_u^* - x_u\|_2 \geq \frac{\|J(x_u)^{\top} \nabla_{\theta} \mathcal{L}(\theta, x_r, y_r)\|_2}{\mu_x \|J(x_u)\|_F + 2\mu_{\theta} \|\nabla_{\theta} \mathcal{L}_u\|_2}.$$

□

C.2 Failure of Classical GIA in Second-Order Federated Unlearning Algorithms

Theorem 4 (Non-Optimality of x_u in Second-Order GIA). *Under Assumptions 5–7, suppose the client's unlearning loss \mathcal{L}_u is defined via a Newton update:*

$$\nabla_{\theta} \mathcal{L}_u = H_r^{-1} \nabla_{\theta} \mathcal{L}(\theta, x_u, y_u),$$

and the server uses a first-order surrogate loss:

$$\nabla_{\theta} \tilde{\mathcal{L}}_u(x) = \nabla_{\theta} \mathcal{L}(\theta, x, y_u).$$

Then the ground truth $x = x_u$ is not a local minimizer of $\mathcal{L}_{\text{sim}} = \|\nabla_{\theta} \mathcal{L}_u - \nabla_{\theta} \tilde{\mathcal{L}}_u(x)\|_2^2$.

Proof. The gradient of \mathcal{L}_{sim} with respect to x is:

$$\nabla_x \mathcal{L}_{\text{sim}} = -2J(x)^{\top} \left(\nabla_{\theta} \mathcal{L}_u - \nabla_{\theta} \tilde{\mathcal{L}}_u(x) \right),$$

where $J(x) = \frac{\partial \nabla_{\theta} \tilde{\mathcal{L}}_u}{\partial x}$ is the Jacobian. At $x = x_u$, we substitute:

$$\nabla_{\theta} \tilde{\mathcal{L}}_u(x_u) = \nabla_{\theta} \mathcal{L}(\theta, x_u, y_u), \quad \nabla_{\theta} \mathcal{L}_u = H_r^{-1} \nabla_{\theta} \mathcal{L}(\theta, x_u, y_u).$$

This gives:

$$\nabla_x \mathcal{L}_{\text{sim}}|_{x=x_u} = -2J(x_u)^{\top} (H_r^{-1} - I) \nabla_{\theta} \mathcal{L}(\theta, x_u, y_u).$$

By Assumption 7, $J(x_u)$ has full column rank. If $H_r^{-1} \neq I$ and $\nabla_{\theta} \mathcal{L}(\theta, x_u, y_u) \neq 0$, the gradient is non-zero. By Fermat's theorem, x_u cannot be a local minimizer. □

Assumption 9. The Hessian H_r is μ_H -Lipschitz in the input, i.e.,

$$\|H_r(x_1) - H_r(x_2)\| \leq \mu_H \|x_1 - x_2\| \quad \forall x_1, x_2.$$

Assumption 10. The inverse Hessian is bounded: $\|H_r^{-1}\| \leq \kappa$.

Theorem 5 (Second-Order Reconstruction Error Bound). *Let x_u^* be a minimizer of \mathcal{L}_{sim} under Assumptions 5–10. Then:*

$$\|x_u^* - x_u\|_2 \geq \frac{\|J^\top H_r^{-1} \nabla_\theta \mathcal{L}(\theta, x_r, y_r)\|_2}{\mu_x \|J\|_F + \mu_H \kappa \|\nabla_\theta \mathcal{L}_u\|_2}.$$

Proof. Define $\Delta x = x_u^* - x_u$. Expand $\nabla_\theta \tilde{\mathcal{L}}_u(x_u^*)$ via Taylor series:

$$\nabla_\theta \tilde{\mathcal{L}}_u(x_u^*) = \nabla_\theta \mathcal{L}(\theta, x_u, y_u) + J(x_u) \Delta x + R,$$

where $\|R\|_2 \leq \frac{\mu_x}{2} \|\Delta x\|_2^2$. Substituting into \mathcal{L}_{sim} :

$$\mathcal{L}_{\text{sim}} = \|H_r^{-1} \nabla_\theta \mathcal{L}(\theta, x_u, y_u) - (\nabla_\theta \mathcal{L}(\theta, x_u, y_u) + J(x_u) \Delta x + R)\|_2^2.$$

Simplify using $\nabla_\theta \mathcal{L}_u = H_r^{-1} \nabla_\theta \mathcal{L}(\theta, x_u, y_u)$:

$$\mathcal{L}_{\text{sim}} = \|(H_r^{-1} - I) \nabla_\theta \mathcal{L}(\theta, x_u, y_u) - J(x_u) \Delta x - R\|_2^2.$$

Using $\|H_r^{-1}\| \leq \kappa$ (Assumption 10) and the Hessian Lipschitz property (Assumption 9):

$$\|R\|_2 \leq \frac{\mu_x}{2} \|\Delta x\|_2^2, \quad \|H_r^{-1} - I\| \leq \kappa + 1.$$

Isolate $\|\Delta x\|_2$ via Cauchy-Schwarz and linearize:

$$\|J^\top H_r^{-1} \nabla_\theta \mathcal{L}(\theta, x_r, y_r)\|_2 \leq (\mu_x \|J\|_F + \mu_H \kappa \|\nabla_\theta \mathcal{L}_u\|_2) \|\Delta x\|_2.$$

Rearranging yields the stated bound. \square

C.3 Correctness of DRAUN for First- and Second-Order Algorithms

As shown previously, classical GIA fails to reconstruct the ground truth unlearn input x_u because the server's surrogate loss $\tilde{\mathcal{L}}_u$ depends only on the dummy unlearn input \tilde{x}_u . This mismatch leads to a biased local minimum of the similarity loss \mathcal{L}_{sim} , especially when the client's unlearning loss \mathcal{L}_u implicitly depends on both x_u and x_r .

To address this, DRAUN incorporates the retain input x_r into the GIA optimization problem. The surrogate loss $\tilde{\mathcal{L}}_u$ is then defined over both dummy inputs $(\tilde{x}_u, \tilde{x}_r)$, making \mathcal{L}_{sim} a function of two variables. Theorems 6 and 7 formalize this intuition by showing that the pair (x_u, x_r) is a local minimizer of the similarity loss under both first-order and second-order formulations.

Theorem 6 (First-Order DRAUN Correctness). *Under Assumptions 5–7, let the client's unlearning loss be:*

$$\nabla_\theta \mathcal{L}_u = \nabla_\theta \mathcal{L}(\theta, x_r, y_r) - \nabla_\theta \mathcal{L}(\theta, x_u, y_u),$$

and the server's surrogate loss be:

$$\nabla_\theta \tilde{\mathcal{L}}_u(\tilde{x}_u, \tilde{x}_r) = \nabla_\theta \mathcal{L}(\theta, \tilde{x}_r, y_r) - \nabla_\theta \mathcal{L}(\theta, \tilde{x}_u, y_u).$$

*Then, the ground truth pair $(\tilde{x}_u, \tilde{x}_r) = (x_u, x_r)$ is a **local minimizer** of:*

$$\mathcal{L}_{\text{sim}}(\tilde{x}_u, \tilde{x}_r) = \left\| \nabla_\theta \mathcal{L}_u - \nabla_\theta \tilde{\mathcal{L}}_u(\tilde{x}_u, \tilde{x}_r) \right\|_2^2.$$

Proof. Compute the gradient of \mathcal{L}_{sim} at $(\tilde{x}_u, \tilde{x}_r)$:

$$\nabla_{\tilde{x}_u, \tilde{x}_r} \mathcal{L}_{\text{sim}} = -2 \begin{bmatrix} J_u^\top \\ -J_r^\top \end{bmatrix} \left(\nabla_\theta \mathcal{L}_u - \nabla_\theta \tilde{\mathcal{L}}_u(\tilde{x}_u, \tilde{x}_r) \right),$$

where $J_u = \frac{\partial \nabla_\theta \mathcal{L}(\theta, \tilde{x}_u, y_u)}{\partial \tilde{x}_u}$ and $J_r = \frac{\partial \nabla_\theta \mathcal{L}(\theta, \tilde{x}_r, y_r)}{\partial \tilde{x}_r}$.

At $(\tilde{x}_u, \tilde{x}_r) = (x_u, x_r)$, we have:

$$\nabla_\theta \tilde{\mathcal{L}}_u(x_u, x_r) = \nabla_\theta \mathcal{L}_u \implies \nabla_{\tilde{x}_u, \tilde{x}_r} \mathcal{L}_{\text{sim}}|_{(x_u, x_r)} = 0.$$

The Hessian at (x_u, x_r) is:

$$\nabla_{\tilde{x}_u, \tilde{x}_r}^2 \mathcal{L}_{\text{sim}}|_{(x_u, x_r)} = 2 \begin{bmatrix} J_u^\top J_u & -J_u^\top J_r \\ -J_r^\top J_u & J_r^\top J_r \end{bmatrix}.$$

By Assumption 7, J_u and J_r have full column rank, so the Hessian is positive definite. Thus, (x_u, x_r) is a local minimizer. \square

Theorem 7 (Second-Order DRAUN Correctness). *Under Assumptions 5–10, let the client’s unlearn loss be:*

$$\nabla_{\theta} \mathcal{L}_u = H_r^{-1} \nabla_{\theta} \mathcal{L}(\theta, x_u, y_u),$$

and the server’s surrogate loss be:

$$\nabla_{\theta} \tilde{\mathcal{L}}_u(\tilde{x}_u, \tilde{x}_r) = \tilde{H}_r^{-1} \nabla_{\theta} \mathcal{L}(\theta, \tilde{x}_u, y_u),$$

*where $\tilde{H}_r = \nabla_{\theta}^2 \mathcal{L}(\theta, \tilde{x}_r, y_r)$. Then, $(\tilde{x}_u, \tilde{x}_r) = (x_u, x_r)$ is a **local minimizer** of:*

$$\mathcal{L}_{\text{sim}}(\tilde{x}_u, \tilde{x}_r) = \left\| \nabla_{\theta} \mathcal{L}_u - \nabla_{\theta} \tilde{\mathcal{L}}_u(\tilde{x}_u, \tilde{x}_r) \right\|_2^2.$$

Proof. At $(\tilde{x}_u, \tilde{x}_r) = (x_u, x_r)$, we have $\tilde{H}_r = H_r$, so:

$$\nabla_{\theta} \tilde{\mathcal{L}}_u(x_u, x_r) = H_r^{-1} \nabla_{\theta} \mathcal{L}(\theta, x_u, y_u) = \nabla_{\theta} \mathcal{L}_u.$$

This implies $\mathcal{L}_{\text{sim}}(x_u, x_r) = 0$. To verify (x_u, x_r) is a local minimizer, compute the gradient and Hessian of \mathcal{L}_{sim} . The gradient is:

$$\nabla_{\tilde{x}_u, \tilde{x}_r} \mathcal{L}_{\text{sim}} = -2 \begin{bmatrix} J_u^{\top} H_r^{-1} \\ -J_r^{\top} H_r^{-1} \end{bmatrix} \left(\nabla_{\theta} \mathcal{L}_u - \nabla_{\theta} \tilde{\mathcal{L}}_u \right),$$

where $J_u = \frac{\partial \nabla_{\theta} \mathcal{L}(\theta, x_u, y_u)}{\partial x_u}$ and $J_r = \frac{\partial \nabla_{\theta} \mathcal{L}(\theta, x_r, y_r)}{\partial x_r}$. At (x_u, x_r) , the term $\nabla_{\theta} \mathcal{L}_u - \nabla_{\theta} \tilde{\mathcal{L}}_u$ vanishes, giving $\nabla_{\tilde{x}_u, \tilde{x}_r} \mathcal{L}_{\text{sim}}|_{(x_u, x_r)} = 0$. The Hessian at (x_u, x_r) is:

$$\nabla_{\tilde{x}_u, \tilde{x}_r}^2 \mathcal{L}_{\text{sim}} \approx 2 \begin{bmatrix} J_u^{\top} H_r^{-2} J_u & 0 \\ 0 & J_r^{\top} H_r^{-2} J_r \end{bmatrix},$$

which is positive definite by Assumption 7 (full column rank J_u, J_r) and Assumption 10 ($H_r \succ 0$). Thus, (x_u, x_r) is a local minimizer. \square

C.4 Bounding Reconstruction Error for First- and Second-Order DRAUN

As discussed in Section 2, DRAUN does not aim to reconstruct the true retain samples x_r . Instead, as described in the initialization step of Algorithm 3, the server simply generates dummy retain inputs of the same size as the unlearn dataset. Although \tilde{x}_r is not meant to match x_r , we aim for it to be close. This motivates the analysis of how proximity to x_r impacts the reconstruction of x_u .

In this section, we provide upper bounds on the reconstruction error $\|\tilde{x}_u - x_u\|$ under both first-order and second-order DRAUN formulations, assuming that the client loss depends on both unlearn and retain inputs.

Assumption 11 (Proximity of Optimized Dummy Inputs). *Let $\tilde{x}_r^{(T)}$ be the dummy retain input after T optimization steps in (Algorithm 1). We assume:*

$$\tilde{x}_r^{(T)} \in B(x_r, \epsilon(T)), \quad \text{where } \epsilon(T) = \mathcal{O}(1/\sqrt{T}),$$

and the gradient $\nabla_{\theta} \mathcal{L}$ is μ_x -Lipschitz in x (per Assumption 8).

Theorem 8 (First-Order Reconstruction Bound). *Under Assumptions 5-8, 11, the reconstruction error after T steps satisfies:*

$$\|\tilde{x}_u^{(T)} - x_u\|_2 \leq \frac{\mu_x \epsilon(T) + \mathcal{L}_{\text{sim}}^{1/2}(T)}{\sigma_{\min}(J_u)},$$

where: $J_u = \frac{\partial \nabla_{\theta} \mathcal{L}(\theta, x_u, y_u)}{\partial x_u}$ with $\sigma_{\min}(J_u) > 0$ (Assumption 7), and $\mathcal{L}_{\text{sim}}(T) = \|\nabla_{\theta} \mathcal{L}_u - \nabla_{\theta} \tilde{\mathcal{L}}_u^{(T)}\|_2^2$ is the similarity loss at step T where $\nabla_{\theta} \tilde{\mathcal{L}}_u^{(T)} = \nabla_{\theta} \mathcal{L}(\theta, \tilde{x}_r^{(T)}, y_r) - \nabla_{\theta} \mathcal{L}(\theta, \tilde{x}_u^{(T)}, y_u)$

Proof. Using μ_x -Lipschitz gradients (Assumption 8):

$$\|\nabla_{\theta} \mathcal{L}(\theta, x_r, y_r) - \nabla_{\theta} \mathcal{L}(\theta, \tilde{x}_r^{(T)}, y_r)\|_2 \leq \mu_x \epsilon(T).$$

Expand the unlearn term around x_u :

$$\nabla_{\theta} \mathcal{L}(\theta, \tilde{x}_u^{(T)}, y_u) = \nabla_{\theta} \mathcal{L}(\theta, x_u, y_u) + J_u(\tilde{x}_u^{(T)} - x_u) + R,$$

with $\|R\|_2 \leq \frac{\mu_x}{2} \|\tilde{x}_u^{(T)} - x_u\|_2^2$. From the similarity objective:

$$\mathcal{L}_{\text{sim}}(T) = \|(\nabla_{\theta} \mathcal{L}(\theta, x_r, y_r) - \nabla_{\theta} \mathcal{L}(\theta, \tilde{x}_r^{(T)}, y_r)) - (J_u(\tilde{x}_u^{(T)} - x_u) + R)\|_2^2.$$

Apply triangle inequality and use $\sigma_{\min}(J_u)$ -lower bound (Assumption 7):

$$\mathcal{L}_{\text{sim}}^{1/2}(T) \geq \sigma_{\min}(J_u) \|\tilde{x}_u^{(T)} - x_u\|_2 - \mu_x \epsilon(T).$$

Rearranging gives the bound. \square

Theorem 9 (Second-Order Reconstruction Error Bound). *Under Assumptions 5-10 and 11, the reconstruction error satisfies:*

$$\|\tilde{x}_u^{(T)} - x_u\|_2 \leq \frac{\kappa(\mu_x \epsilon(T) + \mu_H \epsilon(T)) + \mathcal{L}_{\text{sim}}^{1/2}(T)}{\sigma_{\min}(J_u)},$$

where $\mathcal{L}_{\text{sim}}(T) = \|\nabla_{\theta} \mathcal{L}_u - \nabla_{\theta} \tilde{\mathcal{L}}_u^{(T)}\|_2^2$.

Proof. Let $H_r = \nabla_{\theta}^2 \mathcal{L}(\theta, x_r, y_r)$ and $\tilde{H}_r = \nabla_{\theta}^2 \mathcal{L}(\theta, \tilde{x}_r^{(T)}, y_r)$. By Assumption 9:

$$\|H_r - \tilde{H}_r\| \leq \mu_H \|x_r - \tilde{x}_r^{(T)}\|_2 \leq \mu_H \epsilon(T).$$

Using the matrix inversion identity $A^{-1} - B^{-1} = A^{-1}(B - A)B^{-1}$ and Assumption 10 ($\|H_r^{-1}\| \leq \kappa$):

$$\|H_r^{-1} - \tilde{H}_r^{-1}\| \leq \|H_r^{-1}\| \cdot \|H_r - \tilde{H}_r\| \cdot \|\tilde{H}_r^{-1}\| \leq \kappa \cdot \mu_H \epsilon(T) \cdot \kappa = \kappa^2 \mu_H \epsilon(T).$$

Decompose the gradient difference:

$$\begin{aligned} \nabla_{\theta} \mathcal{L}_u - \nabla_{\theta} \tilde{\mathcal{L}}_u^{(T)} &= \underbrace{(H_r^{-1} - \tilde{H}_r^{-1}) \nabla_{\theta} \mathcal{L}(\theta, x_u, y_u)}_{\text{Hessian error}} \\ &\quad + \underbrace{\tilde{H}_r^{-1} \left(\nabla_{\theta} \mathcal{L}(\theta, x_u, y_u) - \nabla_{\theta} \mathcal{L}(\theta, \tilde{x}_u^{(T)}, y_u) \right)}_{\text{Gradient error}}. \end{aligned}$$

For the Hessian error term:

$$\|(H_r^{-1} - \tilde{H}_r^{-1}) \nabla_{\theta} \mathcal{L}(\theta, x_u, y_u)\|_2 \leq \kappa^2 \mu_H \epsilon(T) \cdot \|\nabla_{\theta} \mathcal{L}(\theta, x_u, y_u)\|_2.$$

By Assumption 8 (μ_{θ} -smoothness), $\|\nabla_{\theta} \mathcal{L}(\theta, x_u, y_u)\|_2 \leq C$ for some constant C , giving:

$$\|\text{Hessian error}\|_2 \leq \kappa^2 \mu_H \epsilon(T) C.$$

For the gradient error term, expand via Taylor series with Jacobian $J_u = \frac{\partial \nabla_{\theta} \mathcal{L}}{\partial x_u}$:

$$\nabla_{\theta} \mathcal{L}(\theta, \tilde{x}_u^{(T)}, y_u) = \nabla_{\theta} \mathcal{L}(\theta, x_u, y_u) + J_u(\tilde{x}_u^{(T)} - x_u) + R,$$

where $\|R\|_2 \leq \frac{\mu_x}{2} \|\tilde{x}_u^{(T)} - x_u\|_2^2$ by Assumption 8. Thus:

$$\|\text{Gradient error}\|_2 \leq \kappa \left(\|J_u(\tilde{x}_u^{(T)} - x_u)\|_2 + \frac{\mu_x}{2} \|\tilde{x}_u^{(T)} - x_u\|_2^2 \right).$$

Combining terms via triangle inequality:

$$\mathcal{L}_{\text{sim}}^{1/2}(T) \geq \sigma_{\min}(J_u) \|\tilde{x}_u^{(T)} - x_u\|_2 - \kappa(\mu_x \epsilon(T) + \mu_H \epsilon(T)).$$

Rearranging yields:

$$\|\tilde{x}_u^{(T)} - x_u\|_2 \leq \frac{\kappa(\mu_x \epsilon(T) + \mu_H \epsilon(T)) + \mathcal{L}_{\text{sim}}^{1/2}(T)}{\sigma_{\min}(J_u)}.$$

\square

C.5 Impact of Initialization Proximity in DRAUN

Assumption 12 (Bounded Reconstruction Step). *The reconstruction step in Algorithm 1 satisfies $\eta_{\text{rec}} \leq \frac{1}{2\mu_x}$, where μ_x is the smoothness constant from Assumption 8.*

Assumption 13 (Proximity at Initialization). *The initial dummy inputs satisfy $\|\tilde{x}_u^{(0)} - \tilde{x}_r^{(0)}\| \leq \Delta$.*

Assumption 14 (Non-Degenerate Gradients). *There exists $c > 0$ such that $\|\nabla_{\theta} \mathcal{L}(\theta, x_u, y_u)\| \geq c$ for all x_u .*

Theorem 10 (Proximity Preservation over Optimization). *Under Assumptions 8 (μ_x -smoothness of \mathcal{L}_{sim}), 12, and 13, after T gradient steps:*

$$\|\tilde{x}_u^{(T)} - \tilde{x}_r^{(T)}\| \leq \Delta \cdot (1 + 2\eta_{\text{rec}}\mu_x)^T.$$

Proof. Let $\delta^{(t)} = \|\tilde{x}_u^{(t)} - \tilde{x}_r^{(t)}\|$. By Assumption 8, the similarity loss gradient satisfies:

$$\|\nabla_{\tilde{x}_u} \mathcal{L}_{\text{sim}}\| \leq \mu_x \delta^{(t)}, \quad \|\nabla_{\tilde{x}_r} \mathcal{L}_{\text{sim}}\| \leq \mu_x \delta^{(t)}.$$

Each gradient update step then obeys:

$$\delta^{(t+1)} \leq \delta^{(t)} + \eta_{\text{rec}} (\|\nabla_{\tilde{x}_u} \mathcal{L}_{\text{sim}}\| + \|\nabla_{\tilde{x}_r} \mathcal{L}_{\text{sim}}\|) \leq \delta^{(t)} (1 + 2\eta_{\text{rec}}\mu_x).$$

Unrolling over T steps yields:

$$\delta^{(T)} \leq \Delta \cdot (1 + 2\eta_{\text{rec}}\mu_x)^T.$$

□

Theorem 11 (First-Order Gradient Collapse). *Under Assumptions 8 (μ_x -smoothness) and $\|J\| \leq C_J$, if $\|\tilde{x}_u - \tilde{x}_r\| \leq \Delta$:*

$$\|\nabla_{\theta} \tilde{\mathcal{L}}_u\| \leq \mu_x \Delta, \quad \|\nabla_x \mathcal{L}_{\text{sim}}\| \leq 2\mu_x C_J \Delta.$$

Proof. By μ_x -Lipschitz continuity (Assumption 8):

$$\|\nabla_{\theta} \tilde{\mathcal{L}}_u\| = \|\nabla_{\theta} \mathcal{L}(\theta, \tilde{x}_r, y_r) - \nabla_{\theta} \mathcal{L}(\theta, \tilde{x}_u, y_u)\| \leq \mu_x \|\tilde{x}_r - \tilde{x}_u\| \leq \mu_x \Delta.$$

The similarity loss gradient becomes:

$$\nabla_x \mathcal{L}_{\text{sim}} = -2J^{\top} (\nabla_{\theta} \mathcal{L}_u - \nabla_{\theta} \tilde{\mathcal{L}}_u),$$

with norm bounded by:

$$\|\nabla_x \mathcal{L}_{\text{sim}}\| \leq 2\|J\| \cdot \|\nabla_{\theta} \mathcal{L}_u - \nabla_{\theta} \tilde{\mathcal{L}}_u\| \leq 2\mu_x C_J \Delta.$$

This implies that as the proximity $\Delta = \|\tilde{x}_u - \tilde{x}_r\|$ approaches zero, the gradient $\nabla_x \mathcal{L}_{\text{sim}}$ vanishes. Consequently, the optimization process may converge prematurely to a false minimum.

□

Theorem 12 (Second-Order Proximity-Inverse Error). *Under Assumptions 9-10, 14, and $\|\tilde{x}_u - \tilde{x}_r\| \leq \Delta$:*

$$\|\tilde{x}_u - x_u\| \geq \frac{\kappa \mu_H c}{\sigma_{\min}(J_u) \Delta + \mu_x},$$

where $\kappa = \|H_r^{-1}\|$, $\sigma_{\min}(J_u) > 0$, and $c > 0$ is from Assumption 14.

Proof. Decompose the gradient mismatch:

$$\nabla_{\theta} \mathcal{L}_u - \nabla_{\theta} \tilde{\mathcal{L}}_u = \underbrace{(H_r^{-1} - \tilde{H}_r^{-1}) \nabla_{\theta} \mathcal{L}(\theta, x_u, y_u)}_{\text{Hessian Error}} + \underbrace{\tilde{H}_r^{-1} J_u e}_{\text{Reconstruction Term}} + \mathcal{O}(\mu_x \|e\|^2),$$

where $e = \tilde{x}_u - x_u$.

By Assumption 9 and Neumann series we have:

$$\|H_r^{-1} - \tilde{H}_r^{-1}\| \geq \frac{\mu_H \Delta}{2\kappa} \implies \|\text{Hessian Error}\| \geq \frac{\mu_H \Delta}{2\kappa} \|\nabla_{\theta} \mathcal{L}\| \geq \frac{\mu_H \Delta c}{2\kappa}.$$

And by Jacobian action:

$$\|\tilde{H}_r^{-1} J_u e\| \leq \frac{\sigma_{\min}(J_u)}{\kappa} \|e\|.$$

From $\mathcal{L}_{\text{sim}} \geq 0$:

$$\frac{\mu_H \Delta c}{2\kappa} \leq \frac{\sigma_{\min}(J_u)}{\kappa} \|e\| + \mu_x \|e\|.$$

Solving for $\|e\|$ gives:

$$\|e\| \geq \frac{\kappa \mu_H c}{2(\sigma_{\min}(J_u) + 2\kappa \mu_x)} \geq \frac{\kappa \mu_H c}{\sigma_{\min}(J_u) \Delta + \mu_x}.$$

□

D Additional Details of Datasets and Models

D.1 Dataset Details

Table 3 lists the datasets used in our experiments. Each dataset was uniformly split across 100 clients, except FEMNIST, which is already partitioned by user.

Table 3: Summary of datasets used in our experiments.

Dataset	Samples	Classes	Input Shape	Description
CIFAR-10	60,000	10	$3 \times 32 \times 32$	Tiny color images of everyday objects
CIFAR-100	60,000	100	$3 \times 32 \times 32$	Similar to CIFAR-10 but with 100 fine-grained classes
MNIST	70,000	10	$1 \times 28 \times 28$	Grayscale handwritten digits (0–9)
FEMNIST	~800,000	62	$1 \times 28 \times 28$	Extended MNIST with digits and letters, partitioned by user

CIFAR-10 and CIFAR-100: Both datasets consist of small natural images from 10 or 100 categories, respectively. The images are RGB, and each has a resolution of 32×32 pixels. CIFAR-10 has 6,000 images per class, while CIFAR-100 provides only 600 per class, making it more challenging due to the finer granularity.

MNIST: MNIST contains grayscale images of handwritten digits from 0 to 9. Each image is 28×28 pixels. The dataset is balanced and often used for benchmarking classification models on simple tasks.

FEMNIST: FEMNIST is an extended version of MNIST built for federated learning. It includes digits (0–9), uppercase (A–Z), and lowercase (a–z) letters, for a total of 62 classes. It is partitioned by writer ID, enabling realistic non-IID client splits in federated settings.

D.2 MLP and ConvNet Model Architecture

In addition to the ResNet18 [21] and LeNet [32] models, we consider two additional neural network architectures: a Multi-Layer Perceptron (MLP) and a deep convolutional network referred to as ConvNet64. The details of these two models are provided in Table 4 and Table 5, respectively

MLP: The MLP consists of three hidden layers, each with width 1024 and ReLU activation functions. The input is first flattened before being passed through fully connected layers. While the base architecture assumes an input shape of $3 \times 32 \times 32$ (for datasets like CIFAR), we adapt the input layer to match the shape of other datasets such as MNIST and FEMNIST, which have smaller grayscale images.

Table 4: Architecture of the MLP model. The input dimension varies depending on the dataset.

Layer	Description
Input	Flatten ($C \times H \times W$)
Linear 1	Linear(input_dim \rightarrow 1024)
ReLU 1	ReLU()
Linear 2	Linear(1024 \rightarrow 1024)
ReLU 2	ReLU()
Linear 3	Linear(1024 \rightarrow 1024)
ReLU 3	ReLU()
Output	Linear(1024 \rightarrow num_classes)

Table 5: Feature extractor architecture of ConvNet64. Width is denoted by w .

Layer	Description
Conv 0	Conv2D($C \rightarrow 1w$), 3×3 , padding=1
BN + ReLU	BatchNorm + ReLU
Conv 1	Conv2D($1w \rightarrow 2w$), 3×3 , padding=1
BN + ReLU	BatchNorm + ReLU
Conv 2	Conv2D($2w \rightarrow 2w$), 3×3 , padding=1
BN + ReLU	BatchNorm + ReLU
Conv 3	Conv2D($2w \rightarrow 4w$), 3×3 , padding=1
BN + ReLU	BatchNorm + ReLU
Conv 4	Conv2D($4w \rightarrow 4w$), 3×3 , padding=1
BN + ReLU	BatchNorm + ReLU
Conv 5	Conv2D($4w \rightarrow 4w$), 3×3 , padding=1
BN + ReLU	BatchNorm + ReLU
MaxPool 0	MaxPool2D(3×3)
Conv 6	Conv2D($4w \rightarrow 4w$), 3×3 , padding=1
BN + ReLU	BatchNorm + ReLU
Conv 7	Conv2D($4w \rightarrow 4w$), 3×3 , padding=1
BN + ReLU	BatchNorm + ReLU
MaxPool 1	MaxPool2D(3×3)

ConvNet64: The ConvNet64 architecture is a deep convolutional network composed of 8 convolutional layers, batch normalization, ReLU activations, and two max pooling layers. The model operates on 2D image inputs with num_channels input channels and uses a base width parameter.

E Additional Reconstruction Results

E.1 Reconstruction on Different Model Architectures

We evaluated DRAUN across various datasets and model architectures. Figures 6, 7, and 8 present single-image reconstructions on the FEMNIST dataset using LeNet [32], the MNIST dataset using an MLP, and the CIFAR-100 dataset using ResNet18 [21], respectively. Higher SSIM and PSNR scores, along with lower LPIPS values, indicate greater similarity to the ground truth. We observe that DRAUN achieves strong reconstructions on simpler models; however, recovering data from gradients becomes increasingly challenging with complex architectures such as ResNet18—an inherited limitation from prior gradient inversion attacks [15].

E.2 Reconstruction for Different Unlearning Step Size

We evaluated DRAUN under the FedAvg protocol, where the client is allowed to perform more than one local optimization step ($\mathcal{E} > 1$). Figures 9 and 10 show DRAUN reconstructions on the CIFAR-10 dataset using the ConvNet64 model for $\mathcal{E} = 2$ and $\mathcal{E} = 4$, respectively, across four

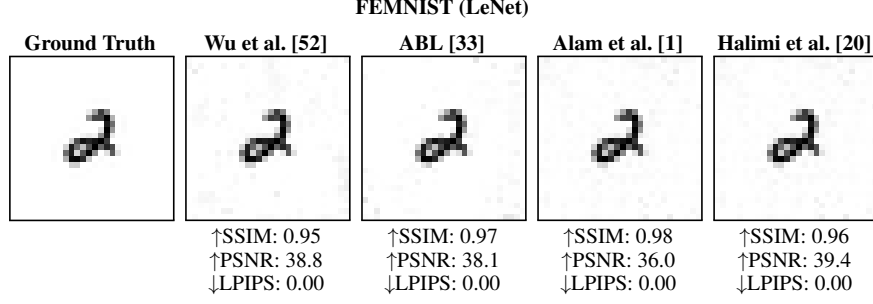


Figure 6: Single-image reconstructions on FEMNIST using LeNet. We compare DRAUN reconstructions from local updates of four unlearning methods. Higher SSIM/PSNR and lower LPIPS indicate better visual fidelity.

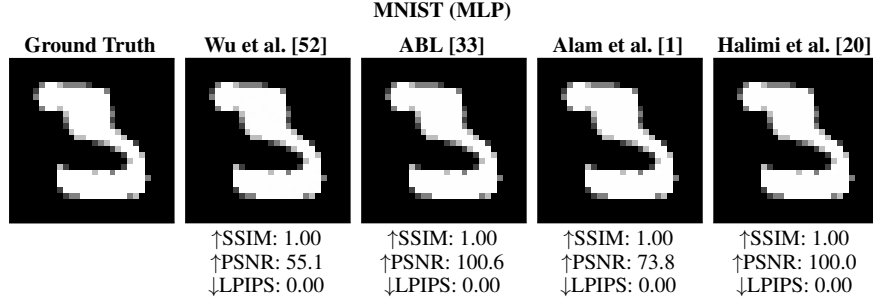


Figure 7: Single-image reconstructions on MNIST using MLP. We compare DRAUN reconstructions from local updates of four unlearning methods.

unlearning algorithms. We observe that reconstruction efficacy deteriorates as the number of local epochs increases.

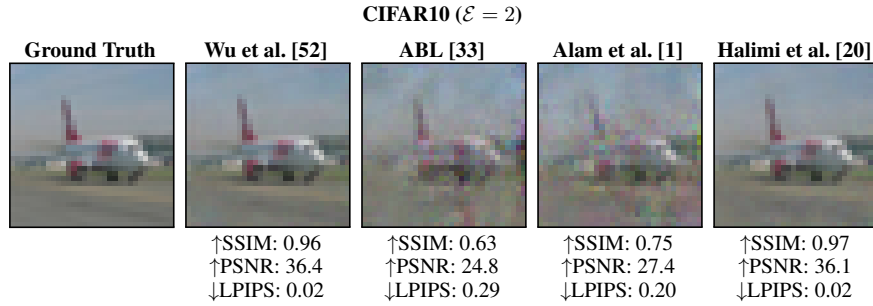


Figure 9: Reconstruction results from local updates with $\mathcal{E} = 2$ steps on CIFAR-10 using ConvNet64. DRAUN is applied to four unlearning methods. Higher SSIM/PSNR and lower LPIPS indicate better reconstruction quality.

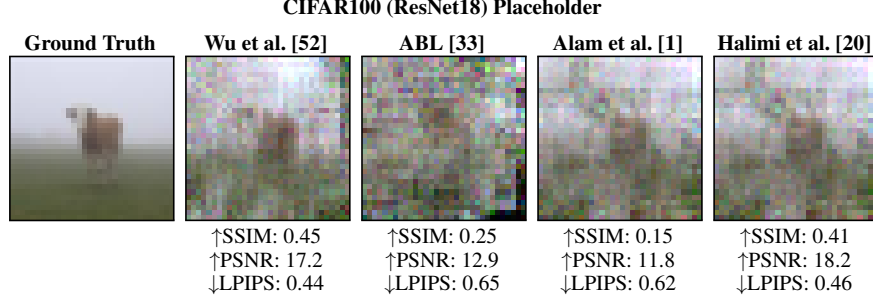


Figure 8: Single-image reconstructions on CIFAR100 using ResNet18. We compare DRAUN reconstructions from local updates of four unlearning methods.

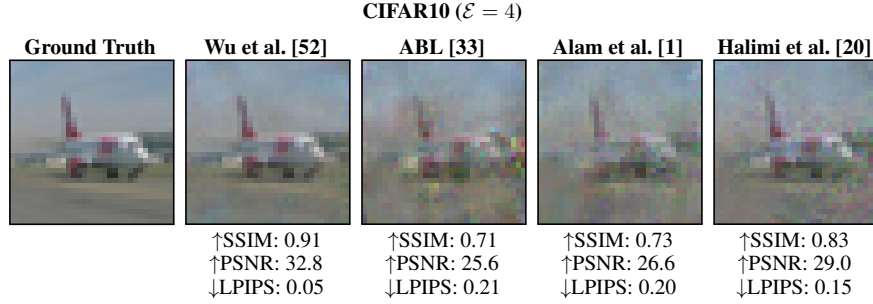


Figure 10: Reconstruction results from local updates with $\mathcal{E} = 4$ steps on CIFAR-10 using ConvNet64. DRAUN is applied to four unlearning methods. Higher SSIM/PSNR and lower LPIPS indicate better reconstruction quality.

E.3 Reconstructed Images for CIFAR100, FEMNIST and MNIST

Figures 11, 12, and 13 demonstrate the capability of DRAUN to reconstruct images across different datasets and unlearning algorithms using the ConvNet64 model.

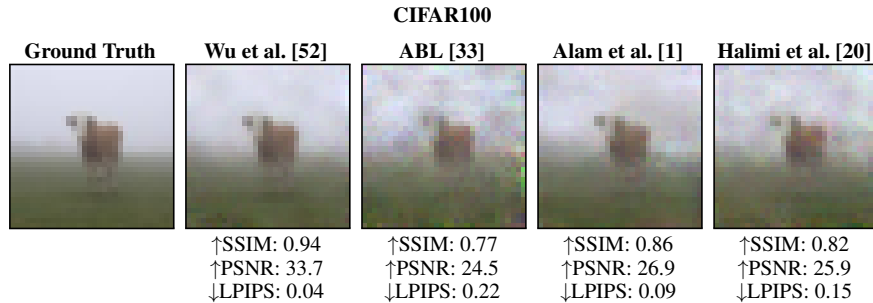


Figure 11: *DRAUN* reconstructions from local updates of four unlearning methods on CIFAR100.

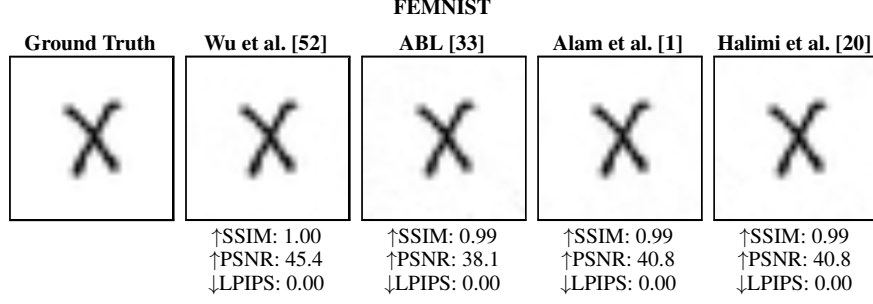


Figure 12: *DRAUN* reconstructions from local updates of four unlearning methods on FEMNIST.

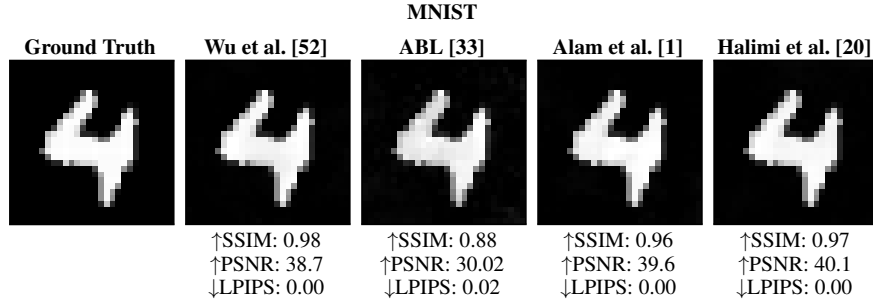


Figure 13: *DRAUN* reconstructions from local updates of four unlearning methods on MNIST.

E.4 Batch Reconstructions for Datasets and Batch Sizes

We evaluate *DRAUN* by reconstructing images from local model updates produced by two unlearning methods—ABL [33] and Halimi et al. [20]—across four datasets: CIFAR-10, CIFAR-100, FEMNIST, and MNIST. Figures 14 to 23 show how reconstruction quality degrades as the batch size of removed samples increases from 4 to 128. While these figures focus on visual results from two representative methods, the accompanying metric plots (Figures 16 to 25) provide a broader comparison across all evaluated algorithms. They show consistent trends—declining SSIM and PSNR, and increasing LPIPS—highlighting the growing difficulty of unlearning larger forget sets.

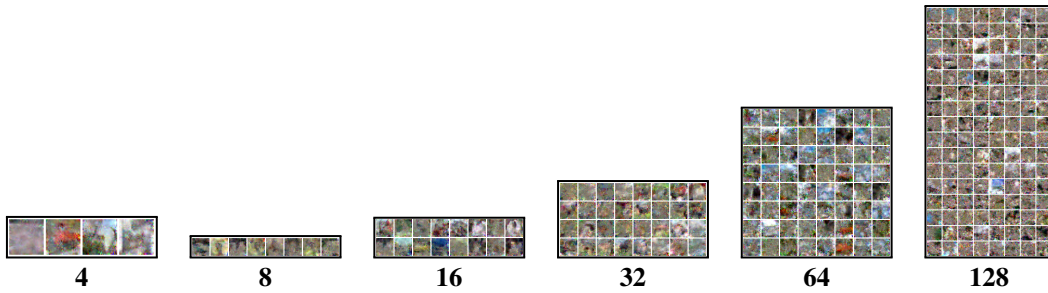


Figure 14: Multi image reconstruction from Halimi et al. [20] on CIFAR10.

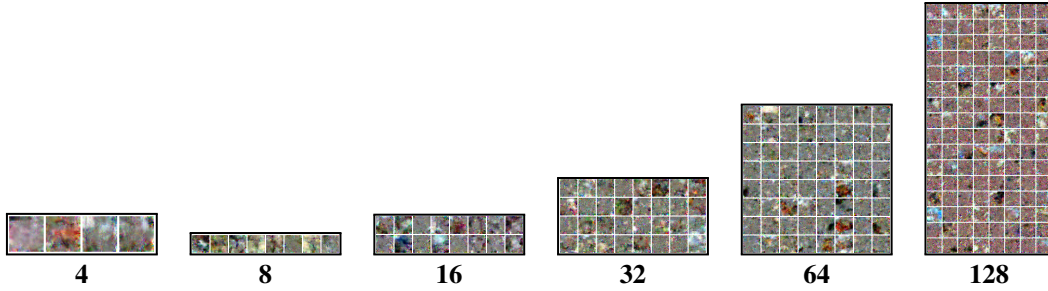


Figure 15: Multi image reconstruction from ABL [33] on CIFAR10.

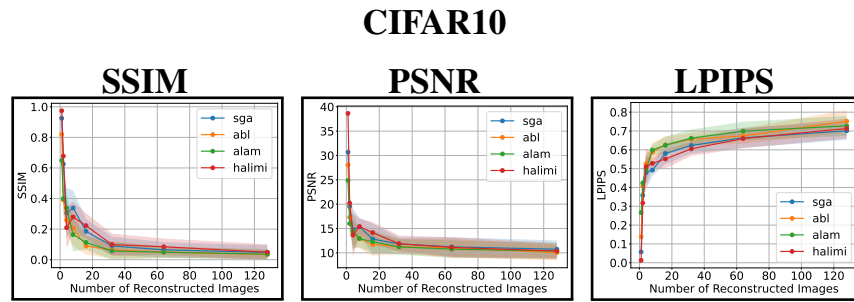


Figure 16: Effect of batch size scaling on reconstruction quality for the CIFAR10 dataset on four unlearning algorithms, measured using SSIM, PSNR, and LPIPS. Larger batch sizes tend to degrade reconstruction fidelity, as indicated by decreasing SSIM/PSNR and increasing LPIPS.

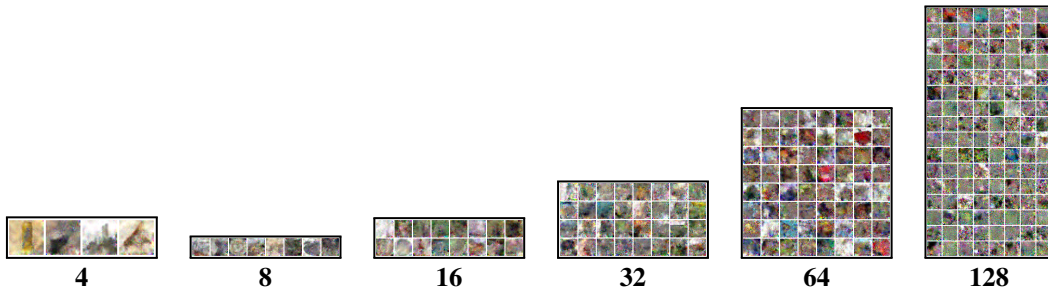


Figure 17: Multi image reconstruction from Halimi et al. [20] on CIFAR100.

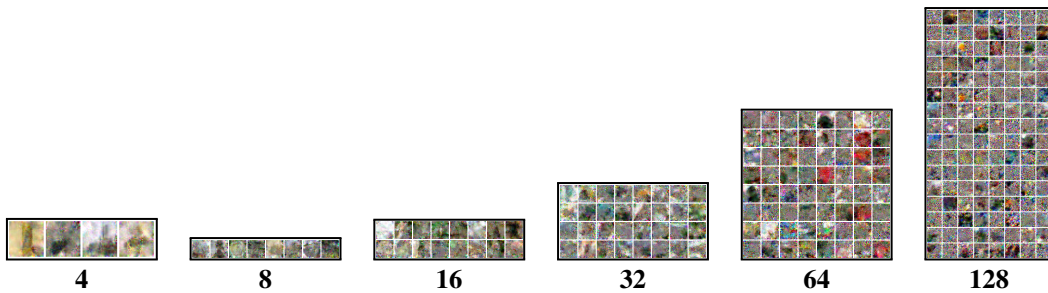


Figure 18: Multi image reconstruction from ABL [33] on CIFAR100.

CIFAR100

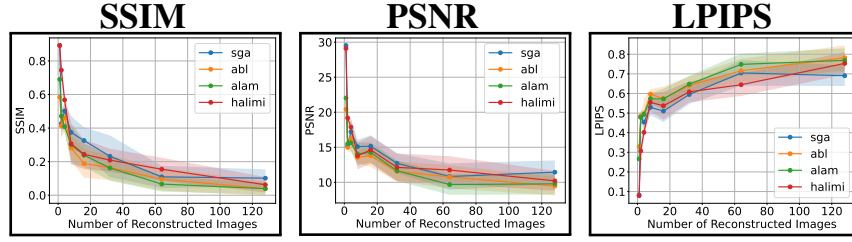


Figure 19: Effect of batch size scaling on reconstruction quality for the CIFAR100 dataset on four unlearning algorithms, measured using SSIM, PSNR, and LPIPS. Larger batch sizes tend to degrade reconstruction fidelity, as indicated by decreasing SSIM/PSNR and increasing LPIPS.

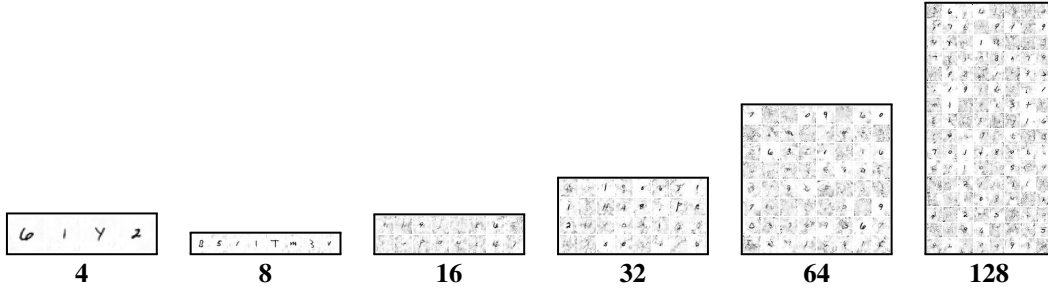


Figure 20: Multi image reconstruction from Halimi et al. [20] on FEMNIST.

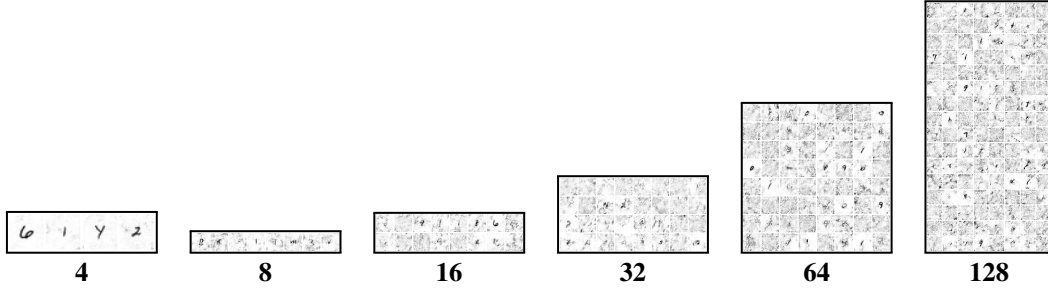


Figure 21: Multi image reconstruction from ABL [33] on FEMNIST.

FEMNIST

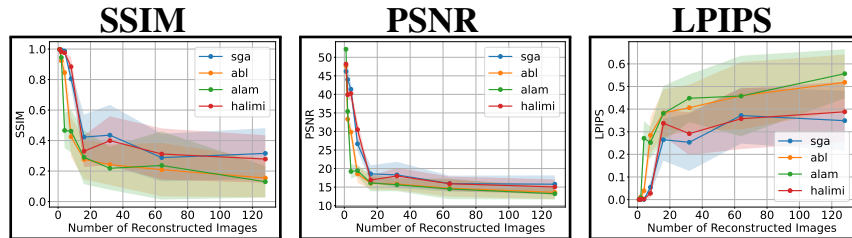


Figure 22: Effect of batch size scaling on reconstruction quality for the FEMNIST dataset on four unlearning algorithms, measured using SSIM, PSNR, and LPIPS. Larger batch sizes tend to degrade reconstruction fidelity, as indicated by decreasing SSIM/PSNR and increasing LPIPS.

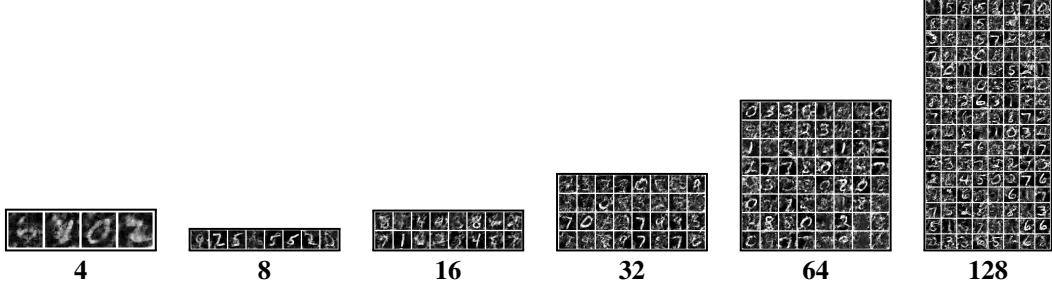


Figure 23: Multi image reconstruction from Halimi et al. [20] on MNIST.

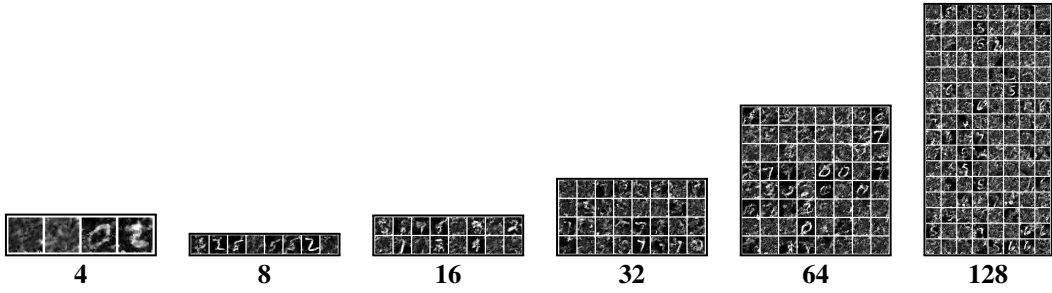


Figure 24: Multi image reconstruction from ABL [33] on MNIST.

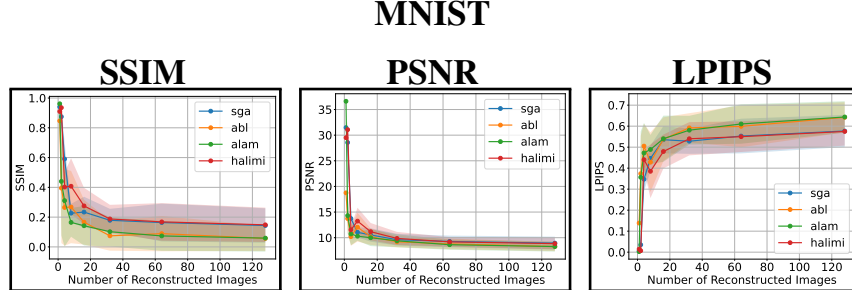


Figure 25: Effect of batch size scaling on reconstruction quality for the MNIST dataset on four unlearning algorithms, measured using SSIM, PSNR, and LPIPS. Larger batch sizes tend to degrade reconstruction fidelity, as indicated by decreasing SSIM/PSNR and increasing LPIPS.

E.5 Reconstruction Comparison between Algorithm-Specific and Algorithm-Agnostic

To evaluate the performance of DRAUN under different unlearning configurations, we compare reconstructions obtained using Alam [1] in both agnostic and specific modes across four datasets: MNIST, FEMNIST, CIFAR-10, and CIFAR-100 (Figures 26–29). While the agnostic mode assumes minimal knowledge about the internal details of the unlearning algorithm, the specific mode leverages full access to its optimization logic and hyperparameters. As expected, the specific setup generally leads to better reconstructions, benefiting from targeted penalties and aligned update dynamics.

CIFAR-10

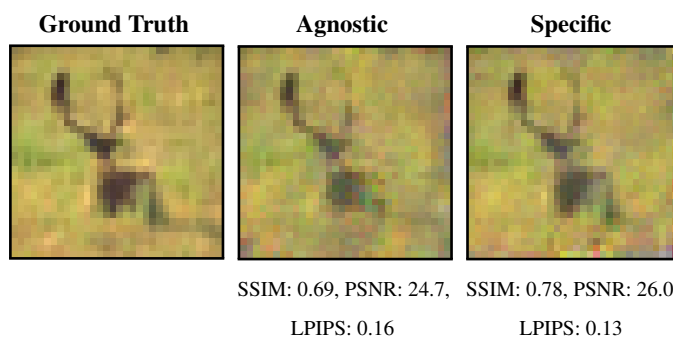


Figure 26: *DRAUN*: Agnostic vs Specific reconstruction on CIFAR-10 using Alam [1] unlearning.

CIFAR-100

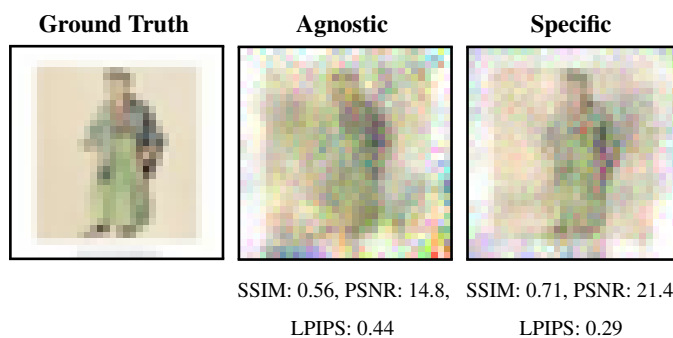


Figure 27: *DRAUN*: Agnostic vs Specific reconstruction on CIFAR-100 using Alam [1] unlearning.

FEMNIST

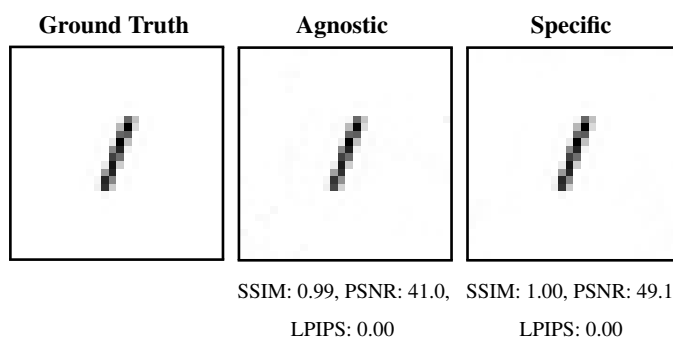


Figure 28: *DRAUN*: Agnostic vs Specific reconstruction on FEMNIST using Alam [1] unlearning.

MNIST

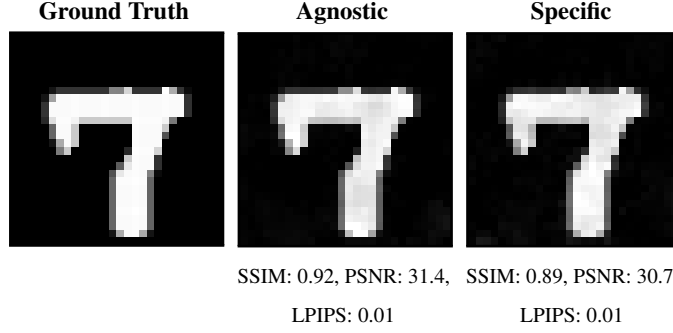


Figure 29: *DRAUN*: Agnostic vs Specific reconstruction on MNIST using Alam [1] unlearning.

F *DRAUN* for Second-Order Unlearning Algorithms

We extend *DRAUN* to the setting where the client employs second-order unlearning algorithms. While uncommon in federated learning due to their high computational cost, Jin et al. [29] show that Newton-style updates can be applied to linearized MLPs. To reconstruct the unlearned data, *DRAUN* generalizes classical gradient inversion attacks by simulating second-order updates on dummy data, as outlined in Algorithm 5. Specifically, the server approximates the client’s update by computing Hessian-vector products (HVPs) using dummy inputs and aligns them with the true HVPs by minimizing their cosine distance. To reduce the computational burden of exact Hessian inversion, we follow the approximation strategy from Zhou et al. [60]. Reconstruction is optimized via SGD with total variation (TV) regularization. For simplicity, we assume access to unlearn labels during reconstruction. Theoretical justifications for the correctness of this approach and the failure modes of classical GIA under second-order updates are provided in Appendix C.

Algorithm 5 *DRAUN* for Second-Order Algorithms

- 1: **Client Input:** Local model θ_c , datasets $(x_u, y_u), (x_r, y_r)$, learning rate η
 - 2: $\nabla \mathcal{L}_u \leftarrow \nabla \mathcal{L}(x_u, y_u; \theta_s)$
 - 3: $H_r \leftarrow H(x_r, y_r; \theta_s)$
 - 4: $\Delta \theta \leftarrow H_r^{-1} \cdot \nabla \mathcal{L}_u$
-
- 5: **Server Input:** Global model θ_s , reconstruction step size η_{rec} , similarity loss \mathcal{L}_{sim} , TV weight λ_{TV}
 - 6: Initialize dummy variables $\tilde{x}_u, \tilde{y}_u, \tilde{x}_r, \tilde{y}_r$ randomly
 - 7: **for** $t = 1$ to T **do**
 - 8: $\nabla \tilde{\mathcal{L}}_u \leftarrow \nabla \mathcal{L}(\tilde{x}_u, \tilde{y}_u; \theta_s)$
 - 9: $\tilde{H}_r \leftarrow H(\tilde{x}_r, \tilde{y}_r; \theta_s)$
 - 10: $\tilde{\Delta} \theta \leftarrow \tilde{H}_r^{-1} \cdot \nabla \tilde{\mathcal{L}}_u$
 - 11: $\ell \leftarrow \mathcal{L}_{\text{sim}}(\Delta \theta, \tilde{\Delta} \theta) + \lambda_{\text{TV}} \cdot \text{TV}(\tilde{x}_u)$
 - 12: $\tilde{x}_u \leftarrow \tilde{x}_u - \eta_{\text{rec}} \cdot \nabla_{\tilde{x}_u} \ell$
 - 13: $\tilde{x}_r \leftarrow \tilde{x}_r - \eta_{\text{rec}} \cdot \nabla_{\tilde{x}_r} \ell$
 - 14: **end for**
 - 15: **return** $(\tilde{x}_u, \tilde{y}_u, \tilde{x}_r, \tilde{y}_r)$
-

G Additional Results on Defense Evaluation against *DRAUN*

We evaluated the effectiveness of pruning and Gaussian noise defenses using the Alam [1] unlearning algorithm on CIFAR-10, with 90 training rounds followed by 10 unlearning rounds. As shown in Figures 30, both defenses introduce a significant drop in model accuracy—on both retained and unlearned data—while only moderately increasing reconstruction difficulty. This illustrates a critical

limitation: although these defenses reduce leakage, their impact on utility renders them unsuitable for practical federated unlearning deployments where accuracy must be preserved.

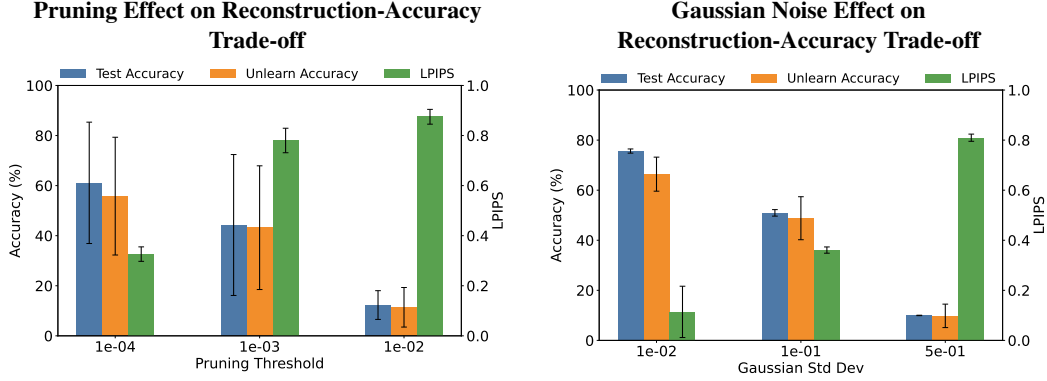


Figure 30: *DRAUN* reconstruction-accuracy trade-off under pruning and Gaussian noise defenses.

H Broader Impacts

Recent works [24, 4] have shown that unlearning algorithms are vulnerable to data reconstruction attacks in Machine Learning as a Service (MLaaS) settings. However, this vulnerability remains unexplored in the context of federated unlearning—a setting where unlearning is critical due to data ownership and regulatory constraints. In this work, we demonstrate that federated unlearning is highly vulnerable when facing a malicious server. In realistic industrial scenarios, such as computer vision classification tasks, we show that the server can silently reconstruct the raw images that a client requests to unlearn—without interfering with the unlearning process. These images are often highly sensitive (e.g., medical X-rays) and typically involve a small number of samples, making accurate reconstruction more feasible. Our findings expose a serious privacy risk in current federated unlearning methods and call for a rethinking of their trust assumptions. We hope this work motivates future research on the privacy-utility trade-offs in federated unlearning, as well as the development of detection and mitigation strategies specifically tailored to this emerging threat model.